



1 **Controls on redox-sensitive trace metals in the Mauritanian oxygen minimum zone**

2 Insa Rapp^{1*}, Christian Schlosser¹, Jan-Lukas Menzel Barraqueta^{1, 2}, Bernhard Wenzel¹, Jan Lüdke¹,
3 Jan Scholten³, Beat Gasser⁴, Patrick Reichert¹, Martha Gledhill¹, Marcus Dengler¹, and Eric P.
4 Achterberg¹

5 ¹Helmholtz Centre for Ocean Research Kiel (GEOMAR), Wischhofstr. 1-3, 24148 Kiel, Germany

6 ²Department of Earth Sciences, Stellenbosch University, Stellenbosch, 7600, South Africa

7 ³Institute of Geosciences, Christian-Albrecht University Kiel (CAU), Otto-Hahn-Platz 1, 24118 Kiel,
8 Germany

9 ⁴International Atomic Energy Agency (IAEA), Environment Laboratories, 4 Quai Antoine 1er, 98012
10 Monaco

11 *Corresponding author. irapp@geomar.de



1 ABSTRACT

2 The availability of the micronutrient iron (Fe) in surface waters determines primary production, N₂
3 fixation and microbial community structure in large parts of the world's ocean, and thus plays an
4 important role in ocean carbon and nitrogen cycles. Eastern boundary upwelling systems and the
5 connected oxygen minimum zones (OMZs) are typically associated with elevated concentrations of
6 redox-sensitive trace metals (e.g. Fe, manganese (Mn) and cobalt (Co)), with shelf sediments typically
7 forming a key source. Over the last five decades, an expansion and intensification of OMZs has been
8 observed and this trend is likely to proceed. However, it is unclear how trace metal (TM) distributions
9 and transport are influenced by decreasing oxygen (O₂) concentrations. Here we present dissolved (d;
10 <0.2 μm) and leachable particulate (Lp; >0.2 μm) TM data collected at 7 stations along a 50 km
11 transect in the Mauritanian shelf region. We observed enhanced concentrations of Fe, Co and Mn
12 corresponding with low O₂ concentrations (<50 μmol kg⁻¹), which were decoupled from major
13 nutrients and nutrient-like and scavenged TMs (cadmium (Cd), lead (Pb), nickel (Ni) and copper
14 (Cu)). Additionally, data from repeated station occupations indicated a direct link between dissolved
15 and leachable particulate Fe, Co, Mn, and O₂. An observed dFe decrease from 10 to 5 nmol L⁻¹
16 coincided with an O₂ increase from 30 to 50 μmol kg⁻¹ and with a concomitant decrease in turbidity.
17 The changes in Fe (Co and Mn) were likely driven by variations in their release from sediment pore
18 water, facilitated by lower O₂ concentrations and longer residence time of the water mass on the shelf.
19 Variations in organic matter remineralization and lithogenic inputs (atmospheric deposition or
20 sediment resuspension) only played a minor role in redox-sensitive TM variability. Vertical dFe fluxes
21 from O₂-depleted subsurface to surface waters (0.08–13.5 μmol m⁻² d⁻¹) were driven by turbulent
22 mixing and vertical advection, and were an order of magnitude larger than atmospheric deposition
23 fluxes (0.63–1.43 μmol m⁻² d⁻¹). Benthic fluxes are therefore the dominant dFe supply to surface
24 waters on the continental margins of the Mauritanian upwelling region. Overall, our results indicated
25 that the projected future decrease in O₂ concentrations in OMZs may result in increases in Fe, Mn and
26 Co concentrations.

27 1. INTRODUCTION

28 The micronutrient iron (Fe) is essential for phytoplankton growth, but due to biological uptake
29 coupled with a low solubility and low supply rates, the availability of Fe is typically low in open
30 ocean surface waters (Bruland and Lohan, 2006). As a result, Fe limits primary production in high
31 nitrate low chlorophyll regions (Boyd, 2007) and regulates dinitrogen (N₂) fixation in (sub)-tropical
32 waters (Moore et al., 2009). Alongside Fe, other trace metals (TMs) such as cobalt (Co), manganese
33 (Mn), zinc (Zn), cadmium (Cd) and copper (Cu) may (co-)limit phytoplankton growth and influence
34 community composition (Browning et al., 2017; Moore et al., 2013; Morel and Price, 2003; Saito et
35 al., 2008).



1 Oxygen minimum zones (OMZs) are characterized by stable subsurface oxygen (O_2) minima, which
2 are maintained by a combination of enhanced O_2 consumption in the thermocline and a limited supply
3 of O_2 rich water masses (e.g. Brandt et al., 2015; Karstensen et al., 2008; Wyrki, 1962). Enhanced O_2
4 consumption is a result of elevated surface productivity caused by upwelling of nutrient-rich
5 subsurface waters in eastern boundary regions of the oceans through Ekman divergence, and intense
6 remineralization of sinking particles (e.g. Helly and Levin, 2004). Elevated organic matter supply and
7 water column O_2 depletion lead to enhanced benthic release of redox-sensitive elements by influencing
8 sediment diagenetic processes (Noffke et al., 2012; Severmann et al., 2010). Elevated concentrations
9 of sediment derived dissolved Fe, Co and Mn have been associated with lateral offshore advection in
10 O_2 depleted waters in the Arabian Sea, Pacific and Atlantic Ocean (Biller and Bruland, 2013; Hatta et
11 al., 2015; Hawco et al., 2016; Milne et al., 2017; Moffett et al., 2015; Noble et al., 2012).

12 Oxygen concentrations affect the distribution of redox-sensitive TMs by controlling oxidation rates
13 and influencing microbially mediated redox transformations. The reduced form of redox-sensitive
14 TMs, such as iron (Fe(II)), cobalt (Co(II)) and manganese (Mn(II)), have a higher solubility in
15 aqueous solutions than their oxidized forms (Fe(III), Co(III), Mn(III/IV)) (Liu and Millero, 2002;
16 Stumm and Morgan, 1995). Reduction of these metals occurs to a large extent in anoxic sediment pore
17 waters by microbial induced dissolution of particulate Fe(III) and Mn(III/IV) oxyhydroxides (Burdige,
18 1993; Chaillou et al., 2002; Froelich et al., 1979). Sediment pore waters are released to overlying
19 bottom waters by diffusion and bio-irrigation and during submarine groundwater discharge (Beck et
20 al., 2007; Elrod et al., 2004; Green et al., 2002). In contact with O_2 and other oxidants (e.g. nitrate
21 (Schlosser et al., 2018) and hydrogen peroxide (Moffett and Zika, 1987)), Fe(II) oxidizes to the poorly
22 soluble Fe(III) species, that are rapidly transformed into amorphous Fe oxyhydroxides or scavenged
23 onto particle surfaces (Moffett and Zika, 1987; Scholz et al., 2016; Wu and Luther, 1994). Mn(II) also
24 oxidizes to insoluble Mn(III/IV) oxides, but due to the slow abiotic oxidation kinetics, especially
25 under low O_2 conditions (e.g. von Langen et al., 1997), biotic oxidation by manganese oxidizing
26 bacteria is the main oxidation mechanism for Mn (Moffett, 1994; Sunda and Huntsman, 1988; Tebo
27 and Emerson, 1986). Co(II) removal is mainly associated with incorporation of Co into Mn oxides by
28 Co co-oxidation (Moffett and Ho, 1996).

29 Stabilizing mechanisms that prevent removal by scavenging and precipitation of Fe, Co and Mn are
30 organic ligand complexation (Elrod et al., 2004; Liu and Millero, 2002; Oldham et al., 2017; Parker et
31 al., 2007) and adsorption onto small slow sinking or neutral buoyant particles (Lam et al., 2012).
32 Recent studies suggest a potentially important role for dynamic exchange processes between dissolved
33 and particulate phases of Fe, thereby influencing cycling and transport (Achterberg et al., 2018;
34 Fitzsimmons et al., 2017; Labatut et al., 2014; Milne et al., 2017). This was further indicated by Fe
35 isotope studies suggesting an equilibrium isotopic fractionation between dissolved and particulate



1 phase in deep waters (Labatut et al., 2014) and the concomitant deepening of the dissolved and
2 particulate Fe plume that originated from a hydrothermal vent (Fitzsimmons et al., 2017).

3 Spatial and seasonal variations in TMs that are released from sediments, as well as ex-situ sediment
4 incubation experiments suggest a direct influence of bottom water and water column O₂ concentrations
5 on the distribution of Fe, Co and Mn (e.g. Biller and Bruland, 2013; Homoky et al., 2012). Differences
6 in benthic TM supply in field studies however are also influenced by a range of other processes as for
7 example sediment type and organic matter supply (Homoky et al., 2016). Ex-situ sediment incubation
8 experiments offer a potential means to disentangle the influence of O₂ concentrations relative to these
9 controls (Homoky et al., 2012). These experiments, however, need to be interpreted within the context
10 of the confined conditions that eliminate potentially important interactions in open systems, such as
11 seawater exchange and mixing. Furthermore, they offer no means to confidently evaluate controls on
12 TM distributions in the pelagic water column.

13 In an attempt to resolve the controls on TM release and stabilization in OMZs we measured the
14 concentration of a suite of TMs along a 50 km long transect on the Mauritanian shelf in the Eastern
15 Tropical North Atlantic (ETNA). The Mauritanian shelf is associated with a major OMZ (minimum O₂
16 concentrations below 40 μmol kg⁻¹; Brandt et al., 2015) and is an important Fe source to the North
17 Atlantic Ocean (Milne et al., 2017). Furthermore, atmospheric dust deposition from the Saharan desert
18 can markedly elevate surface water Fe concentrations in the ETNA (Conway and John, 2014;
19 Rijkenberg et al., 2012). Recent observations suggest a decline in O₂ content of the oceans,
20 particularly in the northern and southern eastern Atlantic, and an expansion of OMZs, modulated by
21 the variability of our climate system (Hahn et al., 2017; Schmidtko et al., 2017; Stramma et al.,
22 2008b). These changes may result in changes in TM supply, and a mechanistic understanding of the
23 factors regulating TM release and stabilization in OMZs is therefore urgently needed. The aim of this
24 study was to evaluate the direct influence of variability in water column O₂ concentrations on the
25 distribution of redox-sensitive TMs and to identify responsible control mechanisms. Firstly, we assess
26 the fluxes of dFe in the OMZ to surface waters by advection and diffusive mixing and compared those
27 to the atmospheric deposition flux of dFe. Secondly, we evaluate the importance of redox and non-
28 redox controls on Fe, Co and Mn by focusing on the influence of O₂ and particles on the distribution
29 of dissolved and leachable particulate TMs, including redox-sensitive (Fe, Co and Mn) and nutrient-
30 type and scavenged trace metals (aluminum (Al), lead (Pb), nickel (Ni), Cd and Cu). Thirdly, we
31 determine the influence of variability of the eastern boundary circulation and O₂ concentrations in
32 regulating TM concentrations.

33 2. METHODS

34 2.1 Sampling



1 Samples were collected on RV Meteor cruise M107 in June 2014 during nine deployments at seven
2 locations (two stations were occupied twice) along a cross-shelf transect at 18°20'N on the
3 Mauritanian shelf in the ETNA (Figure 1). The bottom depths of stations varied between 50 m on the
4 shelf to 1136 m furthest off shore. Seawater sampling was carried out using a trace metal clean CTD
5 (TM-CTD, Sea-Bird SBE25) rosette frame equipped with 24 trace metal clean samplers (12 L, Ocean
6 Test Equipment (OTE)). The CTD frame was attached to plastic coated nonconductive steel cable and
7 deployed using a carousel auto-fire module (AFM, Sea-Bird) that closed the bottles at predefined
8 depths. After recovery, the bottles were transferred to a clean-laboratory container and pressurized to
9 0.2 bar overpressure using filtered N₂ gas. Samples were collected unfiltered for total dissolvable (TD)
10 TM measurements, and filtered using a 0.2 µm cartridge filter (Acropack 500, Pall) for dissolved (d)
11 TMs and iodide. Trace metal samples were collected in acid clean 125 mL low density polyethylene
12 (LDPE) bottles (Nalgene), and iodide samples in opaque 60 mL high density polyethylene (HDPE)
13 bottles (Nalgene). Trace metal samples were acidified to pH 1.9 using ultra clean HCl (UpA, Romil)
14 and stored double-bagged for >6 months before preconcentration and analysis. Samples for iodide
15 measurements were stored frozen at -20°C until analysis.

16 Samples for the determination of radium isotopes (²²³Ra; t_{1/2} = 11.4 d; ²²⁴Ra t_{1/2} = 3.7 d) were obtained
17 using in-situ filtration pumps (Challenger Oceanic) following the procedures described in Charette et
18 al. (2015) and Henderson et al. (2013). Briefly, each in-situ filtration pump was equipped with two
19 particle filters (70 µm; 1 µm) and two Mn dioxide (MnO₂) impregnated cartridges (CUNO Micro
20 Klean III acrylic) on which dissolved Ra adsorbs. The pumped water volumes varied between 1000 L
21 and 1700 L. For the determination of Ra in surface waters (~5 m water depth) about 200–300 L of
22 seawater was pumped into 500 L plastic barrels followed by filtration over MnO₂ coated acrylic fibers
23 (Mn-fibers).

24 2.2 Trace metal analysis

25 Determination of Co, Mn, Fe, Cd, Pb, Ni and Cu was carried out as described in Rapp et al. (2017).
26 Briefly, samples were preconcentrated using an automated preconcentration device (SeaFAST,
27 Elemental Scientific Inc.) equipped with a cation chelating resin (WAKO; Kagaya et al., 2009).
28 Samples were UV-digested prior to preconcentration to breakdown metal-organic complexes, which
29 would cause an underestimation of the determined TM concentrations. Samples were buffered in-line
30 to pH 6.4 ± 0.2 using 1.5 M ammonium acetate buffer, before loading onto the resin. The pH buffer
31 was prepared using an ammonium hydroxide solution (22%, OPTIMA grade, Fisher) and acetic acid
32 (glacial, OPTIMA grade, Fisher) in de-ionized water (MilliQ, Millipore), adjusted to pH 8.5. Retained
33 TMs were eluted from the resin using 1 M distilled HNO₃ and collected in 4 mL polypropylene
34 scintillation vials (Wheaton). The acid was distilled from supra-pure HNO₃ (SpA grade, Romil) using
35 a sub-boiling PFA distillation system (DST-1000, SavilleX). Preconcentration was performed within a
36 clean laboratory (ISO 5) and all sample and reagent handling was performed within the same



1 laboratory in an ISO 3 laminar flow bench with a HEPA filter unit. Preconcentrated samples were
2 analyzed by high resolution inductively coupled plasma-mass spectrometry (HR-ICP-MS, ELEMENT
3 XR, ThermoFisher Scientific) using isotope dilution for Fe, Cd, Pb, Cu and Ni and standard additions
4 for Co and Mn. SAFe reference seawater S and D2 were analyzed with each analytical run and
5 concentrations produced were in good agreement with consensus values (Table 1).

6 Leachable particulate (Lp) concentrations were calculated as the difference between total dissolvable
7 and dissolved concentrations. The limit of quantification (LOQ) for the Lp concentrations was
8 determined as the sum of the analytical standard deviations of TD and dissolved concentrations.
9 Extended uncertainty calculations were performed using the Nordtest approach (Naykki et al., 2015)
10 accounting for random as well as systematic errors (Rapp et al., 2017). The Lp fraction represents the
11 particulate fraction which is readily dissolvable in the acidified samples during storage at pH 1.9 for 6
12 months and therefore does not contain any refractory particle components. This more labile fraction of
13 particulate TMs mainly includes TMs in organic/biogenic particles, adsorbed to particle surfaces and
14 TM oxides/oxyhydroxides (Hurst et al., 2010).

15 **2.3 Aluminum measurements**

16 Aluminum concentrations were determined in surface water samples for all stations along the transect
17 and at two stations (3 and 8) for the entire water column. Samples were analyzed for Al according to
18 Hydes and Liss (1976). Acidified samples were buffered with a 2 M ammonium acetate buffer (Romil,
19 UpA) to a pH between 5.1 and 5.2. Buffered samples were spiked with a 2 mg L⁻¹ lumogallium (TCI)
20 solution. The lumogallium solution was prepared in 2 M ammonium acetate buffer (Romil, UpA).
21 After spiking, samples were heated up for 1.5 h at 80°C in an oven (Heratherm, Thermo Scientific)
22 and left to cool down overnight at room temperature to allow the formation of a fluorescence Al
23 complex. Samples were measured using a fluorescence spectrophotometer (Cary Eclipse, Agilent).
24 The samples were measured with an excitation and emission wavelength of 465 and 555 nm,
25 respectively. All samples were analyzed in duplicate and the concentrations calculated from the peak
26 heights via standard addition. GEOTRACES reference seawater (GS) was run with a mean average
27 Al value of 27.76 ± 0.17 nmol L⁻¹ (n=4; consensus value 28.2 ± 0.2 nmol L⁻¹).

28 **2.4 Iodide measurements**

29 Frozen samples were defrosted overnight at room temperature prior to analysis for iodide by cathodic
30 stripping square wave voltammetry after Luther et al. (1988). The voltammetry unit consisted of a
31 voltammeter stand (663 VA, Metrohm), an autosampler (863 Compact Autosampler, Metrohm) and an
32 automatic burette (843 Pump Station, Metrohm) for automated spike addition. The system was
33 controlled by Computrace software (797 VA; Metrohm).

34

35 **2.5 Oxygen, salinity, nutrient, turbidity and chlorophyll fluorescence analysis**



1 Oxygen, salinity, nutrients, turbidity and chlorophyll fluorescence was measured during 62 CTD
2 deployments (including some repeated deployments at the same location) along the 18°20'N transect
3 using a Sea-Bird SBE 9 CTD rosette system equipped with double sensor packages for O₂, salinity and
4 temperature and 24 niskin samplers (10 L; OTE). Turbidity and chlorophyll a fluorescence were
5 measured with single sensor units on the CTD. Oxygen sensor data were calibrated by Winkler
6 titration (Hansen, 2007; Winkler, 1988) on 348 discrete water samples that were collected from the
7 OTE samplers. The O₂ calibration was undertaken using a linear fit with respect to O₂ concentration,
8 temperature, and pressure. An uncertainty of 1.5 μmol kg⁻¹ was determined. On-board nutrient
9 measurements of nitrite (NO₂⁻), nitrate (NO₃⁻), phosphate (PO₄³⁻) and silicic acid (Si(OH)₄) of the
10 discrete water samples were conducted using a QuAatro autoanalyzer (Seal Analytical) according to
11 Grasshoff et al. (1983).

12 Apparent Oxygen Utilization (AOU) was calculated as the difference between saturation
13 concentrations of O₂ and measured O₂ concentrations. The saturation concentration of O₂ was
14 calculated after the Weiss methods (Weiss, 1970) using the R package marelac (Soetaert et al., 2016),
15 taking into account salinity and temperature.

16 2.6 Radium analysis

17 On-board the ship the Mn-cartridges and Mn-fibers were washed with Ra-free tap water and
18 afterwards partially dried with filtered compressed air to remove excess water. The samples were
19 analyzed for ²²³Ra, ²²⁴Ra and ²²⁸Th using a Radium Delayed Coincidence Counting System (RaDeCC)
20 (Moore and Arnold, 1996). For the efficiency calibration of the RaDeCC, ²²⁷Ac and ²³²Th standard
21 solutions were used, and the calibration followed the procedure described in Scholten et al. (2010) and
22 Moore and Cai (2013). Counting errors were propagated following Garcia-Solsona et al. (2008).
23 Excess ²²⁴Ra (²²⁴Ra_{ex}), i.e. the ²²⁴Ra activity corrected for ²²⁸Th-supported ²²⁴Ra was calculated by
24 subtracting the ²²⁸Th activity from the ²²⁴Ra activity. As we measured only the first Mn cartridge and
25 the Mn cartridges do not adsorb radium quantitatively, we report here only ²²⁴Ra_{ex}/²²³Ra ratios.

26 2.7 Turbulence measurements and vertical flux calculations

27 In order to advance understanding of the role of benthic Fe supply to the high productive surface
28 waters of the upwelling region, vertical diffusive fluxes (eq 1: left term, right hand side) and upwelling
29 induced vertical advective fluxes (eq 1: right term, right hand side) were estimated. At depth in the
30 water on a continental margin, solutes are transferred vertically toward the surface waters by turbulent
31 mixing processes and by vertical advection forced by Ekman divergence (e.g. Steinfeldt et al., 2015):

$$32 \quad J_z = K_z \frac{\partial [TM]}{\partial z} + w \cdot \Delta [TM] \quad (1)$$



1 Here, K_z is the turbulent eddy diffusivity in $\text{m}^2 \text{s}^{-1}$, $\partial[\text{TM}]/\partial z$ the vertical gradient with depth (z) of the
2 TM concentration [TM] in $\mu\text{mol m}^{-3}$, $\Delta[\text{TM}]$ a TM concentration difference in $\mu\text{mol m}^{-3}$ and w
3 represents vertical velocity in m s^{-1} . The equation is solved by vertically integrating the tracer transport
4 budget equation between two vertical layers while ignoring lateral fluxes, changes of w with depth and
5 assuming steady state. Vertical advective fluxes resulting from meso- and submesoscale processes
6 along sloping isopycnals were not considered. The TM-fluxes were evaluated for the depth interval
7 from the upper boundary of the shallow O_2 -depleted waters to a depth of increased chlorophyll a
8 fluorescence (8–29 m depth).

9 Diffusive Fe fluxes were determined by combining TM concentration measurements from the TM-
10 CTD stations with nearby measured microstructure profiles. The microstructure measurements were
11 performed with an MSS90-D profiler (S/N 32, Sea & Sun Technology). The loosely-tethered profiler
12 was optimized to sink at a rate of 0.55 m s^{-1} and equipped with three shear sensors, a fast-response
13 temperature sensor, and an acceleration sensor, two tilt sensors and conductivity, temperature, depth
14 sensors sampling with a lower response time. At TM-CTD stations with bottom depths less than 400
15 m, 18 to 65 microstructure profiles were available at each station. At deeper stations, the number
16 reduced to 5 to 12 profiles. Standard processing procedures were used to determine the rate of kinetic
17 energy dissipation (ϵ) of turbulence in the water column (see Schafstall et al. (2010) for detailed
18 description). Subsequently, K_z values were determined from $K_p = \Gamma \epsilon N^{-2}$ (Osborn, 1980), where N is
19 stratification and Γ is the mixing efficiency for which a value of 0.2 was used. The use of this value
20 has recently shown to yield good agreement between turbulent eddy diffusivities determined from
21 microstructure measurements and from tracer release experiments performed in our study region
22 (Köllner et al., 2016). The 95% confidence intervals for station-averaged K_p values were determined
23 from Gaussian error propagation following Schafstall et al. (2010). Finally, diffusive fluxes were
24 estimated by multiplying station-averaged K_p with the vertical gradient of the respective TM solute,
25 implicitly assuming $K_z = K_p$.

26 The vertical advective flux by Ekman divergence requires determination of vertical velocity in the
27 water column that varies with depth and distance from the coast line. Recent studies found good
28 agreement between vertical velocities derived from Ekman divergence and from helium isotope
29 equilibrium within the Mauritanian and Peruvian coastal upwelling regions (Steinfeldt et al., 2015)
30 when parameterizing vertical velocities as (Gill, 1982):

$$31 \quad w = \frac{\tau_y}{\rho f L_r} e^{-x/L_r}$$

32 where τ_y represents the alongshore wind stress, ρ the density of sea water, x the distance from
33 maximum Ekman divergence taken here as the position at 50 m bottom depth on the shelf and L_r the
34 first baroclinic Rossby radius. The parameterization results from considering the baroclinic response



1 of winds parallel to a coastline in a two-layer ocean (Gill, 1982). The baroclinic Rossby radius
2 $L_r = f^{-1} \sqrt{g \frac{\rho_2 - \rho_1}{\rho} \frac{H_1 H_2}{H_1 + H_2}}$ ($\rho_{1/2}$ and $H_{1/2}$ is density and thickness of the surface and lower layer,
3 respectively) was found to be 15 km from hydrography collected during the cruise, similar to the
4 values determined by Steinfeld et al. (2015) in the same region. Using average alongshore wind stress
5 from satellite data (0.025 Nm^{-2} , ASCAT winds; Ricciardulli and Wentz, 2016) for June 2014,
6 maximum vertical velocities of $3.7 \times 10^{-5} \text{ m s}^{-1}$ were determined for the shelf region (50 m water depth),
7 which decayed offshore to $1.7 \times 10^{-6} \text{ m s}^{-1}$ at the position of the 1000 m isobath at 18°N . As these
8 vertical velocities describe the magnitude of upwelling at the base of the mixed-layer, additional
9 corrections need to be considered for deeper depths. Here, we approximated the vertical decay of w as
10 a linear function which diminishes at the ocean floor.

11 The calculation of the vertical advective flux supplying solutes from the shallow O_2 -depleted waters to
12 the chlorophyll a maximum requires knowledge of a concentration difference $\Delta[\text{TM}]$ associated with
13 the upwelling flux. Ideally, the vertical scale of the concentration difference is determined by
14 correlation analysis of vertical velocity fluctuations and concentration variability at different depths
15 ($w' \cdot [\text{TM}]'$). As these data are not available, we chose to use the mean vertical concentration
16 differences over a vertical distance of 10 m. Thus, the vertical advective flux F_{az} at each station was
17 estimated from $F_{az} = w(x, z) \cdot \frac{\partial[\text{TM}]}{\partial z} 10 \text{ m}$.

18 2.8 Figures

19 All figures were produced in R (version 3.4.3). Data gridding in figures 2 and 3 was performed using
20 the Tps function within the fields package in R (Nychka et al., 2016).

21 3. RESULTS & DISCUSSION

22 3.1 Oceanographic settings of the study area

23 The cruise was conducted in June 2014 along a transect crossing a narrow shelf off the Mauritanian
24 coast at $18^\circ 20' \text{N}$. The vertical structure of the OMZ in this region is characterized by a deep OMZ at
25 about 400 m depth, and a shallow OMZ at about 100 m depth (Brandt et al., 2015). Coastal upwelling
26 of nutrient-rich deep water occurs as a result of offshore transport of surface waters caused by a
27 Northeast Trade wind component parallel to the coast. While north of 20°N upwelling persists
28 throughout the year, upwelling south of 20°N , including the Mauritanian upwelling region, undergoes
29 seasonal changes in upwelling strength (Barton et al., 1998), with strongest upwelling occurring
30 between December and April. The seasonal variability is mainly driven by changes in wind forcing
31 associated with the migration of the Intertropical Convergence Zone (Schafstall et al., 2010).



1 The eastern boundary circulation consists of the Mauritania Current (MC, Fig. 1) flowing poleward at
2 the surface against the equatorward winds and of the Poleward Undercurrent (PUC) flowing in the
3 same direction at depths between 50 and 300 m (Barton, 1989; Klenz et al., 2018; Mittelstaedt, 1983;
4 Peña-Izquierdo et al., 2015). Both currents supply cold, O₂ and nutrient-rich waters of predominantly
5 South Atlantic origin (South Atlantic Central Water, SACW) to the coastal upwelling region (e.g.
6 Mittelstaedt, 1991; Mittelstaedt, 1983; Peña-Izquierdo et al., 2015). In response to the changing winds,
7 the eastern boundary circulation likewise exhibits a pronounced seasonal variability (Klenz et al.,
8 2018; Stramma et al., 2008a). The strongest poleward flow is observed during the relaxation period
9 between May and July when alongshore, upwelling-favorable winds weaken but wind stress curl is at
10 its maximum (Klenz et al., 2018). During the upwelling season in boreal winter, the circulation more
11 closely resembles the classical eastern boundary circulation regime, with a weak poleward
12 undercurrent flowing beneath an equatorward coastal jet. At deeper levels (300–500 m depth), flow
13 was found to be equatorward during both seasons. The shallow (<300 m depth) boundary circulations
14 turn offshore at the southern flank of the Cape Verde frontal zone (CVFZ) (e.g. Tomczak, 1981; Zenk
15 et al., 1991) at about 20°N, separating SACW from more saline and O₂-rich Central Waters formed in
16 the North Atlantic (NACW). The circulation in June 2014 was typical for a relaxation period
17 characterized by little upwelling and a strong poleward flow over the entire shelf between the surface
18 and 250 depth (Klenz et al., 2018).

19 Meridional sections of water mass properties and O₂ concentrations from around 18°N showed that
20 waters with an enhanced SACW proportion advected from the south as well as NACW coming from
21 the north, have higher O₂ concentrations than the ambient waters (Klenz et al., 2018). The mixture of
22 SACW and NACW waters found in the thermocline particularly during boreal winter, previously
23 identified as a regional water mass and termed the Cape Verde SACW (SACW_{cv}) by Peña-Izquierdo
24 et al. (2015), is a signature of an older water mass with lower O₂ concentrations than those of SACW
25 or NACW due to a longer residence time and O₂ consumption through remineralization. Elevated
26 pelagic oxygen consumption levels at the Mauritanian continental margin were recently determined by
27 Thomsen et al. (2018). During the transition period in May through July upper Central Waters (50–
28 300 m depth) are dominated by SACW accounting for 80–90 % of the water masses in the boundary
29 current region (Klenz et al., 2018).

30 The SACW transported poleward within the boundary circulation is supplied by the zonal North
31 Equatorial Counter Current (NECC) and North Equatorial Under Current (NEUC), which flow
32 eastward at about 5°N (Brandt et al., 2015) before diverging into a northward and a southward flowing
33 branch in front of the African coast.

34 As a result of interactions between tidal currents, topography and critically sloping upper continental
35 slope topography (e.g. Eriksen, 1982), the Mauritanian upwelling region is known for elevated
36 nonlinear internal wave activity resulting in enhanced mixing in the water column of the upper slope



1 and shelf region (Schafstall et al., 2010). Vertical fluxes of nutrients driven by mixing processes are
2 amongst the largest reported in literature (Cyr et al., 2015).

3 The CTD and microstructure deployments were performed along the east-west transect in the period
4 June 8 to June 27 (2014) (Fig. 1). Oxygen concentrations reached a deep minimum of 40–50 $\mu\text{mol kg}^{-1}$
5 at about 400 m and a shallow minimum of 30–50 $\mu\text{mol kg}^{-1}$ at about 50–100 m (Fig. 2), which is in
6 agreement with previous studies (Brandt et al., 2015; Thomsen et al., 2018). Mixed layer depths
7 ranged between 10 and 22 m during the cruise. Salinity was highest at the surface (ca. 36.02) and
8 generally decreased with depth to a minimum of 34.71 at around 1000 m. Nitrate (NO_3^-)
9 concentrations in the surface mixed layer varied between 0.1 and 11.3 $\mu\text{mol L}^{-1}$ and phosphate (PO_4^{2-})
10 between 0.15 and 0.91 $\mu\text{mol L}^{-1}$. NO_3^- and PO_4^{2-} concentrations increased with depth to a maximum of
11 47.6 and 3.2 $\mu\text{mol L}^{-1}$, respectively (Fig. 2).

12 Over a time period of 19 days, two trace metal stations were reoccupied along the transect at water
13 depths of 170 m (18.23 °N, 16.52 °W, 1st deployment: June 12, 2nd deployment: June 21) and 189–238
14 m (18.22°N, 16.55°N, 1st deployment: June 24, 2nd deployment: June 26). Minimum O_2 concentrations
15 of 30 $\mu\text{mol kg}^{-1}$ observed before June 15, which increased to 50 $\mu\text{mol kg}^{-1}$ after June 19 or June 24,
16 depending on the location. This oxygenation event that was also captured in ocean glider
17 measurements is discussed in detail by Thomsen et al. (2018). They attributed the change to physical
18 transport of SACW into the region (Thomsen et al., 2018), most likely associated with the observed
19 increase in current speed of the MC flowing northward parallel to the coast line and transporting
20 relatively O_2 -rich water while decreasing the residence time of the SACW along the continental
21 margin. Additionally, pelagic oxygen consumption was found to contribute to the variability in
22 oxygen concentrations close to the seafloor (Thomsen et al., 2018).

23 **3.2 Spatial distributions of dissolved and leachable particulate trace metals**

24 Dissolved Fe and LpFe concentrations ranged between 0.97–18.5 nmol L^{-1} and 1.6–351 nmol L^{-1} ,
25 respectively (Fig. 3a, b). Surface waters (5–29 m) had lowest dFe (0.97–4.7 nmol L^{-1}) and LpFe (1.6–
26 35.9 nmol L^{-1}) concentrations, whereas highest concentrations were present on the shelf close to the
27 seafloor (up to 18.5 nmol L^{-1} dFe and 351 nmol L^{-1} LpFe). Enhanced concentrations of both Fe
28 fractions at any given station were observed at depths with low O_2 concentrations (30–60 $\mu\text{mol O}_2 \text{ kg}^{-1}$)
29 ¹). A similar distribution pattern was observed for dCo, with concentrations between 0.069 and 0.185
30 nmol L^{-1} (Fig. 3c). In contrast, LpCo concentrations varied between below LOQ and 0.179 nmol L^{-1}
31 and were generally highest in surface waters and close to the coast (Fig. 3d). Compared to dFe, the
32 concentration range of dCo was much narrower and enhanced concentrations were observed over a
33 broader depth range and further offshore.

34 Surface dFe and dCo concentrations were low, presumably due to enhanced biological uptake. No
35 clear increasing trend in dFe and dCo with depth was observed, indicating that processes other than, or



1 in addition to, remineralization influenced their distributions. Elevated concentrations were found
2 close to the sediments and within low O₂ waters. This suggested a benthic source of Fe and Co under
3 O₂-depleted conditions, and offshore transport along O₂-depleted water filaments, which is in
4 agreement with previous studies (e.g. Hatta et al., 2015; Hawco et al., 2016; Noble et al., 2012). Our
5 sharper onshore-offshore gradient of dFe concentrations compared to dCo in O₂-depleted waters
6 shows that oxidation and removal mechanisms/scavenging rates were faster for Fe than Co (Noble et
7 al., 2012). Previously reported dFe concentrations in coastal regions of the tropical North Atlantic
8 were lower than we observed, between 0.5–6.3 nmol L⁻¹ (Hatta et al., 2015; Milne et al., 2017).
9 However, all these samples were collected at a greater distance from the coast. In the near-coastal
10 Oregon and Washington shelf bottom water dFe concentrations were similar to our study under
11 equivalent O₂ concentrations (18.7–42.4 nmol L⁻¹ dFe, 42–61 μmol kg⁻¹ O₂; Lohan and Bruland,
12 2008), whereas in the euxinic waters from the Peruvian shelf region, dFe concentrations were more
13 than an order of magnitude higher, exceeding 200 to 300 nmol L⁻¹ (Schlosser et al., 2018; Scholz et al.,
14 2016). Similar dCo concentrations to our study were observed in the North and South Atlantic, with
15 highest concentrations of ~0.16 nmol L⁻¹ present within O₂-depleted waters (Noble et al., 2012; Noble
16 et al., 2017).

17 Dissolved Mn concentrations ranged between 0.46–13.8 nmol L⁻¹ and LpMn between below LOQ–
18 4.4 nmol L⁻¹ (Fig. 3e, f). Highest dMn and LpMn concentrations were observed in surface waters,
19 generally decreasing with depth. Additionally, concentrations were highest on the shelf and decreased
20 offshore. The dMn concentrations were generally elevated within and below the deeper O₂-depleted
21 waters with 0.70–1.34 nmol L⁻¹ compared to 0.46–0.91 nmol L⁻¹ just above. The increased dMn
22 concentrations within the deeper O₂-depleted waters (~350–500 m depth) indicate a benthic source,
23 similar to Fe and Co, which is in accordance with previous studies (Noble et al., 2012). However, in
24 the shallow O₂-depleted waters (~50–200 m depth), this effect is not resolvable due to high surface
25 concentrations, which were maintained by photo-reduction of Mn oxides to soluble Mn(II) that
26 prevents loss of Mn from solution (Sunda and Huntsman, 1994). Reported dMn concentrations in the
27 North and South Atlantic were lower than in our study, with concentrations <3.5 nmol L⁻¹ in surface
28 waters and around 0.5–1 nmol L⁻¹ dMn within the OMZ (Hatta et al., 2015; Noble et al., 2012). As for
29 dFe, these lower reported values can also be explained by sampling stations positioned at further
30 distance from the coast and removal of dMn via biological oxidation processes with distance from the
31 source (Moffett and Ho, 1996).

32 Dissolved Cd and Ni concentrations were lowest in surface waters with 0.022–0.032 nmol Cd L⁻¹ and
33 2.6–2.8 nmol Ni L⁻¹, and showed an increasing trend with depth to maximum values of 0.60 nmol L⁻¹
34 and 5.8 nmol L⁻¹, respectively (Fig. 3g, m). Leachable particulate Cd concentrations were between
35 below LOQ and 0.20 nmol L⁻¹, and LpNi concentrations between below LOQ and 1.7 nmol L⁻¹. A
36 large fraction of Ni (72–100%) was present in the dissolved form. The majority of LpNi samples were



1 below the LOQ (>70% of the data) and LpNi is therefore not included in Fig. 3. LpCd concentrations
2 were highest close to the coast and decreased offshore (Fig. 3h). In surface waters close to the coast
3 the LpCd fraction was dominant with up to 84.3% of the entire Cd pool (d + Lp). The fraction of LpCd
4 in surface water beyond the shelf break (including stations 2, 1 and 9) contributed still up to 54.3% of
5 the Cd pool, whereas below 50 m only 0–12.8% of TDCd was in the Lp phase beyond the shelf break.
6 In contrast to Fe, Co and Mn, no increases in Cd and Ni were observed near the seafloor and within
7 the O₂-depleted waters indicating that Cd and Ni concentrations are mainly controlled by
8 remineralization of sinking organic matter, which is typical for these two nutrient-like TMs (Billier and
9 Bruland, 2013). Similar distributions with concentrations between 0 and 1000 m water depth ranging
10 from ~2–5.5 and ~0–0.55 nmol L⁻¹ for dNi and dCd, respectively, were observed during the
11 GEOTRACES transect GA03_w in the tropical North Atlantic (Mawji et al., 2015; Schlitzer et al.,
12 2018).

13 Dissolved Cu concentrations in surface waters ranged between 0.63–0.81 nmol L⁻¹ (Fig. 3i).
14 Concentrations increased with depth to around 1.37 nmol L⁻¹ at 700 m depth close to the seafloor,
15 whereas highest observed concentrations further offshore were 0.95 nmol L⁻¹ at the greatest sampled
16 depth of 850 m. These results indicate that in addition to remineralization processes of sinking
17 biogenic particles, the distribution of Cu is influenced by inputs from the seafloor. This is in
18 accordance with previous studies, suggesting that Cu is released from continental shelf sediments
19 under oxic and moderately reducing conditions (Billier and Bruland, 2013; Heggie, 1982), whereas no
20 increase in Cu concentrations near the seafloor was observed at low bottom water O₂ concentrations
21 (O₂ <10 μM; Johnson et al., 1988). A decrease in Cu concentrations in the bottom boundary layer was
22 also reported with a seasonal decrease in O₂ in summer from a minimum of 70 μM O₂ in May to 40
23 μM O₂ in August, suggesting a decrease in sedimentary release of Cu (Billier and Bruland, 2013). In
24 strongly reducing sediments and the presence of H₂S, Cu forms inorganic sulfides and precipitates,
25 which may explain reduced sedimentary Cu release under low bottom water O₂ concentrations (Billier
26 and Bruland, 2013). Therefore, the sediment source of dCu might show a different dependency on
27 bottom water O₂ concentrations than dFe, dCo and dMn explaining the distinct distribution of dCu.
28 Concentrations of LpCu were between below the LOQ to 0.61 nmol L⁻¹ with enhanced levels at station
29 4 close to the coast and at mid depths of the three stations furthest offshore (9, 5 and 2) (Fig. 3j).

30 Observed dPb concentrations were lowest in the surface waters at 9–14 pmol L⁻¹ and increased with
31 depth to 29–86 pmol L⁻¹ below 600 m depth (Fig. 3k). Lead is not considered a nutrient-like TM (e.g.
32 Boyle et al., 2014), but our observations indicate a release of Pb from sinking particles following
33 remineralization. The concentration range and depth distribution is similar to reported distributions
34 further offshore at about 21°W (Noble et al., 2015). These authors suggested that increased
35 concentrations of up to 70 pmol L⁻¹ between 600 and 800 m depth were related to the influence of
36 Mediterranean Outflow Waters (MOW). Additionally, increased Pb concentrations in proximity to



1 sediments have been attributed to the benthic release of historic Pb through reversible scavenging from
 2 particles and the release of dPb associated with Fe/Mn oxyhydroxides during reductive dissolution of
 3 those oxides in anoxic sediments (Rusiecka et al., 2018). The major source of Pb to the ocean is
 4 atmospheric dust deposition from anthropogenic emissions (Bridgestock et al., 2016; Nriagu and
 5 Pacyna, 1988; Veron et al., 1994) with a recent indication of reduced anthropogenic Pb inputs to
 6 surface waters in the eastern tropical Atlantic under the North African dust plume (Bridgestock et al.,
 7 2016). Low surface water concentrations on the Mauritanian shelf indicate low atmospheric inputs of
 8 Pb to this region. LpPb was below the LOQ—27 pmol L⁻¹, and the distribution of LpPb was similar to
 9 that of LpFe, with subsurface maxima within O₂-depleted waters (Fig. 3l) and may indicate increased
 10 scavenging of dPb in these layers which might be associated with Fe containing particles.

11 In general, sediment derived TM concentrations decrease with distance from the shelf and with time
 12 that passed since the water mass has been in contact with the sediments due to water mass mixing and
 13 removal processes such as precipitation and scavenging (Bruland and Lohan, 2006). Radium isotopes
 14 can be used as a tracer for benthic sources. The major source of Ra to the ocean is input from
 15 sediments through the efflux of pore water, sediment resuspension, and submarine groundwater
 16 discharge (Moore, 1987; Moore and Arnold, 1996; Rama and Moore, 1996). Due to the distinctive
 17 half-lives of the different Ra isotopes (e.g. ²²⁴Ra (t_{1/2} = 3.66 d) and ²²³Ra (t_{1/2} = 11.4 d)) and their
 18 conservative behaviour in seawater, it is possible to quantify the time that has passed since a parcel of
 19 water was in contact with the sediments using the following equation by Moore (2000):

$$\left(\frac{A_{224}}{A_{223}}\right)_{obs} = \left(\frac{A_{224}}{A_{223}}\right)_i \frac{e^{-\lambda_{224}\tau}}{e^{-\lambda_{223}\tau}} \quad (2)$$

20 solved for water mass age (τ):

$$\tau = \frac{\ln\left(\frac{A_{224}}{A_{223}}\right)_{obs} - \ln\left(\frac{A_{224}}{A_{223}}\right)_i}{\lambda_{223} - \lambda_{224}} \quad (3)$$

21 where A_{224}/A_{223} is the activity ratio of ²²³Ra and ²²⁴Ra, with the subscript *obs* for the observed seawater
 22 ratio and the subscript *i* for the initial groundwater endmember ratio, and λ_{223} and λ_{224} are the decay
 23 constants in d⁻¹ for ²²³Ra and ²²⁴Ra.

24 Highest ²²⁴Ra_{ex}/²²³Ra activity ratios were observed close to the seafloor (Fig. 3n). The average
 25 ²²⁴Ra_{ex}/²²³Ra ratio in proximity to the sediment source (< 20 m above seafloor) was 4.1 ± 0.7 and was
 26 similar to reported ratios for shelf waters off South Carolina (²²⁴Ra_{ex}/²²³Ra = 4.1 ± 0.7; Moore, 2000).
 27 The ²²⁴Ra_{ex}/²²³Ra ratios decreased away from their benthic source due to decay (²²⁴Ra_{ex}/²²³Ra = 0–0.5
 28 in surface waters). Ratios close to the seafloor were relatively constant along the transect at bottom
 29 depths <600 m, whereas dFe, dCo and dMn concentrations varied largely in the bottom samples. This
 30 suggests that factors, which are not influencing the Ra distribution, impacted the distributions of dFe,



1 dCo and dMn, with a likely influence of enhanced O₂ concentrations reducing sediment release or
2 increasing removal rates of these metals at water depths between 200 and 400 m. At around 800 m
3 bottom depth, ²²⁴Ra_{ex}/²²³Ra ratios were slightly elevated and coincided with increased dCo, dFe, dMn
4 and dCu concentrations despite O₂ concentrations >70 μmol kg⁻¹. This suggests that the enhanced TM
5 concentrations at this location were influenced by a strong sediment source which may be related to
6 the presence of a benthic nepheloid layer as indicated by an increase in turbidity in proximity to the
7 seafloor. An elevated ²²⁴Ra_{ex}/²²³Ra ratio of 3.5 ± 0.6 was observed at about 16.65°N and 80 m water
8 depth (bottom depth 782 m) and coincided with a local maximum of dFe, dMn and dCo and reduced
9 O₂ concentrations. These observations indicate that the waters with the local maximum of dFe, dMn
10 and dCo have been in relatively recent contact (12–20 days assuming initial pore water ²²⁴Ra_{ex}/²²³Ra
11 ratios between 18–38; Moore, 2007) with sediments, likely originated from south of our transect as a
12 result of a strong poleward flow (Klenz et al., 2018), and that the dynamic current system in this
13 region can cause local and short-term variability in the transport of sediment derived TMs.

14 3.3 Classification of different groups of trace metals based on principal component analysis

15 Principal Component Analysis (PCA) was performed (using the RDA function within the vegan
16 package in R; Oksanen et al., 2017) to investigate different groups and correlations in the data set.
17 Dissolved TMs (Fe, Mn, Co, Ni, Pb, Cu and Cd), nutrients (silicic acid, nitrate and phosphate),
18 dissolved O₂, Apparent Oxygen Utilization (AOU), depth and iodide concentrations were utilized in
19 the PCA. Radium data were not included in the PCA, as the number of available data points for
20 ²²⁴Ra_{ex}/²²³Ra was much lower than for the other parameters. Surface waters shallower than 50 m were
21 excluded from the PCA to remove the influence of local processes in surface waters, such as localized
22 atmospheric deposition and photochemical processes, which in particular influence Mn and iodide
23 distributions. The PCA generated three principal components (PC) with eigenvalues larger than 1,
24 with PC1 explaining 53.6% and PC2 25.5% of the total variance in the dataset (together 79.1%).
25 Inclusion of PC3 in the analysis explained only 6.8% more of the variance.

26 The first PC group is formed by dCd, dCu, dNi and dPb (Fig. 4), which are associated with depth,
27 AOU, nitrate and phosphate. This indicates that the distribution of Cd, Cu, Ni, and potentially Pb, are
28 controlled by organic matter remineralization processes. This is in agreement with strong Pearson
29 correlations R >0.9 for the relationships of dCd and dNi with depth, nitrate and silicic acid
30 (Supplementary Material, Table S1). Weaker correlations with major nutrients were observed for dPb
31 (R >0.6) and dCu (R >0.4), potentially due to additional remineralization or removal mechanisms for
32 these elements (e.g. prior atmospheric inputs and water mass transport, Pb; sediments, Cu and Pb, and
33 scavenging). The second group of TMs is composed of dFe, dCo and dMn that are associated with
34 elevated iodide and turbidity, and low dissolved O₂ (Fig. 4). Iodide (I) is the reduced form of iodine
35 (I), which is typically present as iodate (IO₃⁻) in oxygenated subsurface water. Both I forms are present
36 as soluble anions in seawater. Due to a relatively high redox potential (pE ~10), iodine is one of the



1 first redox-sensitive elements to undergo reduction under suboxic conditions and is therefore a useful
2 indicator for active reductive processes (Rue et al., 1997). Despite their role as micronutrients, Fe, Mn
3 and Co do not correlate with nutrients indicating that processes other than remineralization controlled
4 their distributions.

5 The anti-correlation with O₂ (also shown in Fig. S1) and correlation with iodide support the notion that
6 Fe, Co and Mn distributions were strongly influenced by water column O₂ concentrations, presumably
7 through: (i) enhanced benthic metal fluxes from anoxic sediments, and (ii) decreased oxidation rates in
8 the overlying water column under O₂-depleted conditions. This is also supported by elevated benthic
9 Fe(II) fluxes observed at the seafloor within the shallow OMZ, with benthic fluxes of 15–27 μmol m⁻²
10 d⁻¹ (Schroller-Lomnitz et al., 2018).

11 Variability in the redox-sensitive metals, Fe, Mn and Co, were not fully explained by either O₂ or
12 iodide concentrations; Pearson correlations with O₂ were -0.55, -0.61 and -0.58, respectively
13 (Supplementary Material, Table S1). As shown before, other factors such as, for example, water mass
14 mixing and age, the amount and type of particles present, and remineralization all likely impact their
15 dissolved concentrations. Consequently, such a complex chain of factors and processes means that one
16 variable alone is unlikely to explain the behaviour of Fe, Mn, and Co.

17 **3.4 Influence of the different sources of Fe, Mn and Co**

18 The main sources of TMs in our study region are sedimentary release and atmospheric dust deposition
19 (e.g. Rijkenberg et al., 2012). Also release of TMs via organic matter remineralization may have an
20 important influence on the distribution of TMs. In the following, we discuss the relative influence of
21 remineralization, atmospheric dust deposition and sedimentary release on the supply of Fe, Co and Mn
22 to surface waters.

23 *3.4.1 Remineralization*

24 To quantify the influence of remineralization for dFe, we employed dFe to carbon (dFe/C) ratios
25 (carbon was calculated using AOU, with an AOU/carbon ratio of 1.6; Martin et al., 1989). Surface
26 data, where O₂ was over-saturated (due to biological O₂ production), were excluded. Dissolved Fe/C
27 ratios for the entire transect varied between 15 and 74 μmol mol⁻¹. These results agree with those for
28 shelf-influenced waters with dFe/C ratios of 13.3–40.6 μmol mol⁻¹ further south at 12°N (Milne et al.,
29 2017). Reported ratios for the North Atlantic, further away from the shelf were lower and ranged
30 between 4 and 12.4 μmol mol⁻¹ (Fitzsimmons et al., 2013; Milne et al., 2017; Rijkenberg et al., 2014).
31 To estimate the amount of dFe being derived by remineralization, we assume a dFe/C ratio of 4–12
32 μmol mol⁻¹ from organic matter remineralization, similar to the observed dFe/C ratios in the open
33 ocean close to our study area without a strong shelf influence. These offshore ratios may still be
34 influenced by an atmospheric source of dFe, which would result in an overestimation of dFe/C ratios



1 from remineralization and thereby an overestimation of the fraction of remineralized dFe. Apart from
2 additional inputs, the dFe/C ratios are influenced by the respective Fe/C stoichiometry in the sinking
3 organic matter and removal of dFe by scavenging. Furthermore, it is not clear if the offshore ratios can
4 be transferred to a location close to the coast, as the balance between remineralization and scavenging
5 processes might be different due to differences in phytoplankton productivity and particle load. Hence,
6 this approach only provides a broad estimate of the relative influence of remineralization on the
7 distribution of dFe in the study area.

8 We obtain a range between $5 \pm 3\%$ and $54 \pm 27\%$ for dFe being derived from remineralization
9 processes with lowest values observed on the shelf at 34 m depth at station 4 ($5 \pm 3\%$) and highest
10 values estimated beyond the shelf break at Stn 9 at 213 m depth ($54 \pm 27\%$) and Stn 2 at 450 m depth
11 ($52 \pm 26\%$). However, no clear increase in the contribution of remineralized dFe to total dFe with
12 depth or distance to the coast was observed. For example at depths between 35 and 200 m, our
13 estimates of dFe from remineralization ranged between $10 \pm 5\%$ and $51 \pm 25\%$ with high values of up
14 to $41 \pm 20\%$ at 50 m depth at station 7 close to the coast, whereas relatively low values of $19 \pm 9\%$
15 were observed at 89 m at station 2. These results indicate that, locally, remineralization can be an
16 important control on dFe concentrations, but that the contribution varies largely with additional
17 important controls, often dominating over remineralization.

18 Similar analysis for dCo/C ratios revealed an increased importance of an additional source close to the
19 shelf. Observed dCo/C ratios ranged between 0.81 and $2.2 \mu\text{mol mol}^{-1}$. The larger ratios were
20 observed close to the coast and decreased further offshore. Overall, the observed ratios were somewhat
21 higher than reported cellular ratios of phytoplankton in the North Atlantic of $0.5\text{--}1.4 \mu\text{mol mol}^{-1}$
22 (Twining et al., 2015). However, relatively constant dCo/C ratios beyond the shelf break (dCo/C:
23 $0.82\text{--}1.09 \mu\text{mol mol}^{-1}$, stations 2, 5 and 9) that are similar to cellular ratios of phytoplankton suggest a
24 large influence of remineralization on dCo beyond the shelf break, whereas enhanced ratios close to
25 the coast suggest an additional benthic source. Due to the lack of comparable data of offshore dCo/C
26 ratios and the multiple processes influencing this ratio (varying phytoplankton nutrient stoichiometry
27 and scavenging), we did not use these values to estimate the remineralized dCo fraction.

28 The distribution of Mn was not predominantly determined by biological uptake and remineralization
29 processes in our study region. In contrast, dMn/C ratios were largely influenced by photoreduction in
30 the surface (Sunda and Huntsman, 1994), removal via biotic oxidation and formation of Mn oxides at
31 depth (Tebo et al., 2004). Therefore, we did not assess remineralization processes for Mn using dMn/C
32 ratios.

33 3.4.2 Atmospheric deposition

34 Aluminum is present as a relatively constant fraction of $\sim 8.15 \text{ wt}\%$ in the continental crust (Rudnick
35 and Gao, 2006), is supplied to open ocean surface waters mainly by atmospheric deposition (Orians



1 and Bruland, 1986) and is considered not to be taken up by phytoplankton (apart from a small amount
2 being incorporated into siliceous diatom frustules; Gehlen et al., 2002). Therefore, dAl in the surface
3 mixed layer is used as a tracer for atmospheric deposition to the surface ocean (Measures and Brown,
4 1996; Measures and Vink, 2000). The atmospheric input in the study region is mainly influenced by
5 North African/Saharan mineral dust with only a small contribution of anthropogenic sources which
6 differ greatly in TM composition and solubilities from mineral dust (Baker et al., 2013; Patey et al.,
7 2015; Shelley et al., 2015). Close to continental shelves, in addition to atmospheric input, Al can also
8 be supplied by sediment resuspension (Menzel Barraqueta et al., 2018; Middag et al., 2012; Moran
9 and Moore, 1991).

10 Our dAl concentrations in surface water ranged between 30 and 49 nmol L⁻¹ and LpAl between 3.4
11 and 18.2 nmol L⁻¹. Dissolved Al concentrations decreased with depth (Fig. 8), indicating that Al was
12 released by aeolian dust deposition to surface waters and removed through scavenging at depth
13 (Orlans and Bruland, 1985). Trace metal (Fe, Co, and Mn) to Al ratios were utilized to investigate the
14 influence of atmospheric dust deposition. We present molar ratios for dissolved (dTM/dAl), total
15 dissolvable (TDTM/TDAI) and leachable particulate (LpTM/LpAl) concentrations. In the surface
16 mixed layer, dFe/dAl molar ratios ranged between 0.019 and 0.114, TDFe/TDAI between 0.236 and
17 0.826 and LpFe/LpAl between 1.04 and 9.50.

18 Literature particulate Fe/Al ratios from aerosol samples collected in the remote North Atlantic
19 between 8.7°N and 23°N were in the range of 0.31 ± 0.06 (Buck et al., 2010; Patey et al., 2015) and
20 0.37 ± 0.02 in the North East Atlantic ~18°N under the Saharan dust plume (Shelley et al., 2015). In
21 contrast, upper crustal material ratios are lower ranging from 0.19 to 0.23 suggesting a slight Fe
22 enrichment of aeolian mineral dust particles (McLennan, 2001; Rudnick and Gao, 2006; Wedepohl,
23 1995). Lower Fe than Al solubilities from aerosol leach experiments in ultra-high purity water (UHP)
24 and 25% acetic acid (HAc) and seawater have been reported (Baker et al., 2006; Buck et al., 2010;
25 Shelley et al., 2018), but soluble Fe/Al ratios from these experiments varied dependant on the leach
26 medium (UHP: 0.21 ± 0.04 , 25% HAc: 0.25 ± 0.04 , seawater: 0.051 ± 0.009 ; Shelley et al., 2018).
27 This indicates that dFe/dAl and LpFe/LpAl ratios in seawater from atmospheric deposition are likely
28 to be lower than particulate ratios of digested aerosol samples in the study region.

29 Our dFe/dAl ratios at the upper end (dFe/dAl: 0.114) are larger than aerosol leaches in seawater
30 indicating a potential additional input of dFe, whereas our lower dFe/dAl ratios than reported ratios in
31 aerosol leaches suggest removal of dFe by biological uptake or scavenging. Our LpFe/LpAl are all
32 larger than reported ratios in aerosol leaches and total aerosol ratios, which shows that there is an
33 additional source of LpFe or transfer of sediment-derived dFe onto the particulate phase by biological
34 uptake or sorption to particles. Total dissolvable ratios comprise both dissolved and leachable
35 particulate phases, thereby being independent of the phase transfer from dissolved to particulate phase
36 (via biological uptake or sorption). The lower end of total dissolvable ratios (TDFe/TDAI: 0.236) were



1 close to the total ratios in aerosol samples, suggesting that atmospheric deposition represented an
2 important source of Fe and Al to the surface ocean. At the upper end, ratios were much larger
3 (TDFe/TDAI: 0.826) than aerosol ratios and indicate an additional benthic source of Fe.

4 These interpretations only apply, however, if residence times of dissolved and particulate Fe and Al
5 phases supplied via atmospheric deposition are similar. This is difficult to assess, as estimated
6 residence times for both elements are dependent on input and removal rates and vary largely between
7 locations. Overall, our Fe/Al ratios suggest that atmospheric deposition is an important source of Fe to
8 surface waters with an additional contribution of benthic inputs. However, uncertainties in solubilities
9 and residence times cause a high uncertainty in the interpretation of the role of atmospheric deposition.

10 Observed dCo/dAl ratios in the upper 50 m were 0.001–0.004, TDCo/TDAI ratios were slightly higher
11 at 0.003–0.005 and LpCo/LpAl ratios were 0.006–0.020. Cobalt is present in the upper continental
12 crust in a much smaller molar fraction than Fe (Co/Al: 0.000071–0.000097; McLennan, 2001;
13 Rudnick and Gao, 2006; Wedepohl, 1995). However, ratios in aerosol samples under the North
14 African dust plume were slightly higher (Co/Al: 0.00016 ± 0.00002 ; Shelley et al., 2015) than crustal
15 ratios and solubility of Co from these aerosol samples was much higher than Al solubility resulting in
16 soluble Co/Al of 0.0021 ± 0.0009 in UHP (Shelley et al., 2018). The soluble ratios also varied largely
17 depending on the leach medium and might therefore also vary from the actual aerosol solubility in
18 seawater at our study site. Our ratios of all fractions were larger than total aerosol ratios and mostly
19 higher than soluble ratios from aerosol leaches. This indicates that an additional benthic source of Co
20 likely contributed to the Co present in surface waters.

21 Dissolved Mn/dAl ratios in the upper 50 m ranged between 0.082 and 0.347, and TDMn/TDAI
22 between 0.083 and 0.256. The ratios are much larger than upper crustal ratios (Mn/Al: 0.0032–0.0037;
23 McLennan, 2001; Rudnick and Gao, 2006; Wedepohl, 1995) but similar to the soluble ratios of Mn/Al
24 from aerosols in UHP (Mn/Al: 0.24 ± 0.09 ; Shelley et al., 2018) indicating that a large amount of Mn
25 may be derived from atmospheric deposition. However, these ratios are heavily overprinted by the
26 long residence time of Mn in surface waters due to photoreduction. Therefore, it is not possible to
27 reliably estimate the contribution of atmospheric Mn deposition based on the Al data.

28 Atmospheric dFe fluxes were calculated using the dAl inventory in the surface mixed layer, a
29 residence time of dAl of 0.65 ± 0.45 years as reported for the Canary Current System (Dammshäuser
30 et al., 2011), and a ratio of 0.31 for dust derived dissolved Fe/Al (Buck et al., 2010). This approach
31 assumes that dAl is only supplied to the surface ocean via atmospheric deposition. Vertical fluxes of
32 Al from sediment resuspension are unlikely to largely contribute to concentrations of dAl in surface
33 waters here as dAl concentrations were decreasing with depth. Mean atmospheric dFe fluxes of the
34 individual stations were 0.63–1.43 $\mu\text{mol m}^{-2} \text{d}^{-1}$ (Fig. 5, Supplementary Table S2), values similar to
35 reported fluxes close to our study region of 2.12 $\mu\text{mol m}^{-2} \text{d}^{-1}$ further north between 22.5–25°N and



1 26.5–27.5°W (Rijkenberg et al., 2012) and $0.120 \text{ nmol m}^{-2} \text{ d}^{-1}$ around 20°N close to the African coast
2 (Ussher et al., 2013). The uncertainty in the residence time of dAl, however, creates a large
3 uncertainty in calculated fluxes resulting in a lowest flux of $0.37 \text{ } \mu\text{mol m}^{-2} \text{ d}^{-1}$ when using the largest
4 estimated residence time of 1.1 years and a highest flux of $4.65 \text{ } \mu\text{mol m}^{-2} \text{ d}^{-1}$ when using the shortest
5 estimated residence time of 0.2 years.

6 3.4.3 Vertical trace element fluxes to surface waters

7 The vertical fluxes (diffusive and advective) of dFe from the top of the shallow O₂-depleted waters
8 (between 23 and 89 m depending on station) into surface waters were determined to assess the
9 potential Fe contribution to phytoplankton growth. A detailed summary of calculated fluxes, the
10 contribution of diffusive and advective term and uncertainties for dFe for all stations is given in
11 Supplementary Information Table S2. Closest to the shelf (bottom depth: 50 m) mean dFe fluxes were
12 $13.5 \text{ } \mu\text{mol m}^{-2} \text{ d}^{-1}$. Further offshore, vertical dFe fluxes decreased to $0.16 \text{ } \mu\text{mol m}^{-2} \text{ d}^{-1}$ (station 2,
13 bottom depth: 1136 m, 77 km offshore) (Fig. 5). However at station 5 higher dFe fluxes were observed
14 (dFe: $1.3 \text{ } \mu\text{mol m}^{-2} \text{ d}^{-1}$) than at stations 9 (closer to the shelf) and 2 (further offshore). At station 5,
15 eddy diffusivity was determined from only 5 microstructure profiles and was unusual high at this
16 station. Therefore, the enhanced vertical fluxes are likely caused by a rare elevated mixing event and
17 do not represent a long-term average. Between repeat stations 3A and 3B, mean fluxes decreased from
18 2.3 (Stn 3A) to $1.35 \text{ } \mu\text{mol m}^{-2} \text{ d}^{-1}$ (Stn 3B), which was partly caused by a difference in the vertical
19 concentration gradient of dFe and partly by a change in diffusivity.

20 On the shelf (station 4, bottom depth: 45 m), dFe fluxes were dominated by vertical advective rather
21 than diffusive fluxes due to the strong upwelling velocity on the shelf (Table S2). At the continental
22 slope stations (stations 3, 7 and 8, bottom depth: 90–400 m), fluxes were dominated by high diffusive
23 fluxes, which were around 3 times larger than the advective flux term. Further offshore (stations 2 and
24 9, bottom depth: >400 m) the contribution of advective and diffusive fluxes were similarly low except
25 for station 5 with particularly strong vertical mixing. Similar vertical dFe ($16 \text{ } \mu\text{mol m}^{-2} \text{ d}^{-1}$) to the
26 upper water column were reported on the shelf at 12°N (Milne et al., 2017). Although, in the study
27 region atmospheric fluxes of dFe were enhanced relative to global averages (Mahowald et al., 2009)
28 with mean fluxes of $0.63\text{--}1.43 \text{ } \mu\text{mol m}^{-2} \text{ d}^{-1}$, our vertical dissolved Fe fluxes from the shallow O₂
29 depleted waters of $0.95\text{--}13.5 \text{ } \mu\text{mol m}^{-2} \text{ d}^{-1}$ exceeded atmospheric fluxes at all stations apart from
30 station 2 ($0.16 \text{ } \mu\text{mol m}^{-2} \text{ d}^{-1}$) furthest offshore and potentially station 9 ($0.08 \text{ } \mu\text{mol m}^{-2} \text{ d}^{-1}$), where no
31 atmospheric fluxes were determined. The weaker influence of atmospheric deposition in this region
32 close to the coast is in accordance with previous studies that demonstrated sediments to be the major
33 contributor to the Fe inventory in the coastal region of the eastern tropical Atlantic, whereas the
34 importance of atmospheric inputs increases further offshore (Milne et al., 2017). Our vertical
35 advective fluxes are likely lower than the annual average and also lower than usually during the
36 relaxation period as upwelling favourable winds were particularly low in June 2014.



1 Dissolved Co fluxes ranged between 2 and 113 $\text{nmol m}^{-2} \text{d}^{-1}$. These values are lower than reported
2 upwelling fluxes of dCo of 250 $\text{nmol m}^{-2} \text{d}^{-1}$ for this region (Noble et al., 2017), but are larger than
3 atmospheric deposition fluxes of 1.7 $\text{nmol m}^{-2} \text{d}^{-1}$ (Shelley et al., 2015). Fluxes of dMn are downwards
4 from surface waters to O₂ depleted waters due to higher concentrations in surface waters.

5 **3.5 Removal mechanisms and particle interactions**

6 In the top 50 m of the water column a large part of the LpTMs may be part of living biological cells
7 (e.g. phytoplankton) or organic detritus. Additionally, LpTMs may be part of lithogenic phases from
8 Saharan dust and sediment particles, or authigenic phases. Authigenic phases are formed in-situ by
9 TM adsorption onto particle surfaces or by the formation of amorphous TM oxides and hydroxides
10 (e.g. FeO(OH) in the mineral structure of goethite) (Sherrell and Boyle, 1992).

11 Iron was mainly present in the size fraction $>0.2 \mu\text{m}$ with TDFe concentrations being 0.44–44.5 times
12 higher than dFe ($<0.2 \mu\text{m}$) (Fig. 6a). To investigate the influence of particle load on the distribution
13 between dissolved and particulate phases, the fraction of Lp (Lp/TD) TMs and Lp concentrations are
14 plotted against turbidity for Fe, Co and Mn (Fig. 6b, c). A low fraction of LpFe of around 60% was
15 observed at lowest turbidity. As turbidity increases from 0.1 to 0.2 NTU, the LpFe fraction increased
16 to $>90\%$. This suggests that the fraction of LpFe is tightly coupled to the particle load. Iron adsorption
17 onto particles has been demonstrated to be reversible with a constant exchange between dissolved and
18 particulate fractions (Abadie et al., 2017; Fitzsimmons et al., 2017; John and Adkins, 2012; Labatut et
19 al., 2014). Furthermore, offshore transport of acid-labile Fe particles originating from reductive
20 dissolution processes from continental shelf sources was observed in the North Pacific (Lam and
21 Bishop, 2008) and may contribute to the bioavailable Fe pool. Therefore an important fraction of Fe
22 may be transported offshore adsorbed to particles and can enter the dissolved pool by cycling between
23 dissolved and particulate phases.

24 Manganese and Co mainly occurred in the dissolved form. The LpCo fraction ranged between 0 and
25 75%, and the fraction and concentration of LpCo, showed linear increases with turbidity, indicating an
26 influence of particle load on Co size fractionation, similar to Fe. In contrast to Fe and Co, the fraction
27 of LpMn varied between 3 and 40%, and did not show a correlation with turbidity, whereas LpMn
28 concentrations showed an increase with turbidity. This indicates that an increased presence of particles
29 coincided with enhanced LpMn levels, but that the particle load did not substantially influence the
30 distribution between dMn and LpMn phases and that particles did not contribute to the dMn fraction.
31 This suggests that particles did not play a major role in transport of dMn, which agrees with a study on
32 hydrothermal vent plumes, where the distribution of the dMn plume was decoupled from the
33 distribution of the particulate Mn plume (Fitzsimmons et al., 2017).

34 The increase in LpFe concentrations with increasing turbidity was weaker in the surface waters
35 compared to water depths below 50 m (Fig. 6c). This suggests a large additional LpFe source at depth



1 with either a higher Fe content of particles or the presence of different sizes of particles causing
2 different responses in turbidity measurements. The large additional LpFe source at depths is likely
3 associated with benthic dFe inputs, with a subsequent transfer to the particulate phase by adsorption or
4 oxidation with subsequent formation of Fe(oxihydr)oxides. Enhanced turbidity at depth may also
5 indicate sediment resuspension, which would result in the release of TM-containing particles from
6 sediments and enhanced release of dTMs from sediment pore water. The effect of sediment
7 resuspension is discussed in more detail below (section 3.6.2).

8 In contrast to Fe, the increase in LpCo and LpMn concentrations with turbidity was similar in surface
9 waters and below and suggests less variability in the composition of the particulate Co and Mn phase
10 throughout the water column with a potentially weaker influence of sediment release on the
11 distribution of particulate Mn and Co. A weaker influence of sediment release might be influenced by
12 a weaker release of Co and Mn from sediments in the dissolved form and slower oxidation rates
13 compared to Fe, in particular for Co (Noble et al., 2012), resulting in a slower conversion into the
14 particulate phase. Such an interpretation based on turbidity data alone, however, is very hypothetical
15 and would require further investigation of particulate TM species composition in this area.

16 **3.6 Temporal variability in redox-sensitive trace metals**

17 Large temporal changes in O₂, turbidity and redox-sensitive TMs were observed within a short time
18 scale of a few days at two repeat stations, station 3A/3B and station 8A/8B (Fig. 7).

19 Station 3 and 8 were sampled twice with a period of nine days between both deployments for station 3
20 (Fig. 7a) and two days for station 8 (Fig. 7b). At station 3, O₂ concentrations in the upper 50 m were
21 very similar between both deployments, whereas below 50 m O₂ increased from 30 μmol kg⁻¹ during
22 the first deployment to 50 μmol kg⁻¹ nine days later. At the same time, turbidity below 50 m had
23 decreased from 0.35 to below 0.2, and dFe concentrations from a maximum of 10 nmol L⁻¹ to 5 nmol
24 L⁻¹ nine days later. In addition, dMn and dCo concentrations decreased from 5 to 3 nmol L⁻¹ and 0.14
25 to 0.12 nmol L⁻¹, respectively. Particularly large changes were also observed for LpTM concentrations
26 with a decrease from 147–322 nmol L⁻¹ to 31–51 nmol L⁻¹ for LpFe, from 0.066–0.114 nmol L⁻¹ to
27 0.015–0.031 nmol L⁻¹ for LpCo and from 1.24–2.64 to 0.16–0.54 for LpMn. In contrast, no changes in
28 water mass properties (T/S) occurred below 50 m (Fig. 7a).

29 Similar changes in O₂ and turbidity were observed at station 8. During the first deployment a local
30 minimum in O₂ below 30 μmol kg⁻¹ was present between 105 m and 120 m water depths which
31 coincided with a maximum in turbidity of 0.4 (Fig. 7b). In contrast O₂ concentrations and turbidity
32 during the second deployment were relatively constant (50–60 μmol kg⁻¹ O₂ and turbidity 0.2) below
33 50 m. At depth of the local O₂ minimum and turbidity maximum, concentrations of dFe, dMn and dCo
34 were elevated during the first deployment with concentrations of 9.4 ± 2.1 nmol dFe L⁻¹, 3.7 ± 0.6



1 nmol dMn L⁻¹ and 0.145 ± 0.033 nmol dCo L⁻¹ in comparison to 4.6 ± 1.0 nmol dFe L⁻¹, 2.6 ± 0.5
2 nmol dMn L⁻¹, and 0.122 ± 0.028 nmol dCo L⁻¹ at similar depth during the second deployment.

3 3.6.1 Remineralization

4 We compared the results of the redox-sensitive TMs to other nutrient-like TMs and PO₄. For both
5 repeat stations only small changes in dCd (Stn 3A: 0.107–0.231 nmol L⁻¹; Stn 3B: 0.135–0.150 nmol
6 L⁻¹) and PO₄ (Stn 3A: 1.59–1.85 μmol L⁻¹; Stn 3B: 1.55–1.71 μmol L⁻¹) concentrations were observed
7 below 50 m (Fig. 8), suggesting that only a small fraction of dFe under lower O₂ conditions was
8 supplied by more intense remineralization of biogenic particles in the water column.

9 A weak influence of remineralization processes on the variability in dFe concentrations was confirmed
10 by substantially higher dFe/C ratios at lower O₂ concentrations (40–72 μmol mol⁻¹ at Stn 3A compared
11 to 33–41 μmol mol⁻¹ at Stn 3B, both below 50 m water depth). Assuming a dFe/C ratio of around 12
12 (see section 3.4.1) from remineralization, only about 0.25 nmol L⁻¹ of the difference in dFe
13 concentrations between repeated deployments can be explained by the difference in remineralization,
14 suggesting that most of the difference in dFe between deployments was caused by changes in source
15 inputs, such as enhanced sediment release during lower bottom water O₂ concentrations, or slower
16 removal by oxidation under lower O₂ conditions.

17 In contrast, dCo/C ratios were similar between repeat deployments within the OMZ (0.90–1.04 at Stn
18 3A and 0.92–1.06 μmol mol⁻¹ at Stn 3B). Thus, changes in remineralization could be a reason for the
19 changes in observed dCo concentrations during repeated deployments, indicating that the sensitivity of
20 dCo sediment input or change in oxidation rates is low at an O₂ shift from 30 to 50 μmol kg⁻¹.

21 Similar to Fe, higher dMn/C ratios were observed at lower O₂ concentrations (3.4–5.5 μmol mol⁻¹ at
22 Stn 3A compared to 2.1–2.9 μmol mol⁻¹ at Stn 3B). These results indicate that other processes than
23 remineralization are also important for the change in dMn concentrations. An additional factor
24 compared to Fe, might involve changes in intensity of photoreduction which may be influenced by
25 differences in surface turbidity observed at station 3 (lower dMn/C and higher surface turbidity during
26 second deployment). This, however, cannot explain the changes in dMn/C at station 8, where a higher
27 surface turbidity coincided with a higher dMn/C ratio at the local minimum in O₂.

28 3.6.2 Atmospheric dust deposition and sediment resuspension

29 Within the OMZ at station 3 and 8, dAl concentrations ranged between 10 and 15 nmol L⁻¹, and LpAl
30 concentration between 1.2 and 11.1 nmol L⁻¹ and no substantial changes were observed between
31 deployments (Fig. 8). As lithogenic material has a high Al content, no substantial changes in Al
32 concentrations signify that lithogenic inputs did not differ much between the deployments.
33 Consequently neither increased atmospheric input, nor sediment resuspension are likely to explain the
34 differences in turbidity and redox-sensitive TM concentrations. Hence, changes in turbidity may



1 mainly have been caused by biogenic particles, such as resuspended organic matter (Thomsen et al.,
2 2018). This finding can be confirmed by substantial changes in TM/Al ratios observed during the
3 deployments (Table 2 and Fig. S2). The Fe/Al ratios in the solid phase of underlying sediments during
4 the cruise were 0.23–0.30 (Schroller-Lomnitz et al., 2018) with Mn/Al ratios of 0.0015–0.0020
5 (Schroller-Lomnitz, pers. com.). Slight increases in LpAl towards the sediment indicate some
6 influence of sediment resuspension on the TM distribution. Overall much higher TM/Al ratios
7 compared to ratios in the sediments and aerosol samples from this region (Fe/Al: 0.37 ± 0.02 , Co/Al:
8 0.00016 ± 0.00002 , Mn/Al: 0.0061 ± 0.0002 ; Shelley et al., 2015), suggest a large additional source of
9 Fe, Co and Mn in the OMZ close to the shelf. This again points towards a large influence of benthic
10 release of Fe, Co and Mn from sediment pore waters and subsequent partial adsorption to particle
11 surfaces.

12 3.6.3 Other possible causes for TM variability

13 From the comparison above, we can conclude that the variations in Fe concentrations during repeated
14 deployments were not caused by increased remineralization or changes in lithogenic inputs from
15 atmospheric deposition or sediment resuspension. The large changes in the Lp fractions must therefore
16 be of biogenic or authigenic origin. If all LpCo would be present in biogenic particles of suspended
17 phytoplankton cells, at our observed maximum of $0.114 \text{ nmol L}^{-1}$ LpCo at station 3A we would expect
18 around 4.6 nmol L^{-1} LpFe in sinking phytoplankton, using an average Fe/Co ratio in phytoplankton of
19 40 (Moore et al., 2013) (observed ratios close to our study area were 20–40; Twining et al., 2015).
20 However, LpFe concentrations were 322 nmol L^{-1} and thereby 70 times larger than our estimate in
21 biogenic particles (4.6 nmol L^{-1}), revealing that the majority of LpFe must be authigenically formed.
22 Altogether our results suggest that changes in particle load as indicated by changes in turbidity do not
23 comprise a major source of dFe, moreover a sink of previously dissolved Fe. Therefore, higher
24 dissolved and Lp concentrations during the first deployment with lower O_2 concentrations must be
25 caused by a stronger benthic source of dissolved Fe.

26 It is not possible to extract from our data whether the stronger benthic source under low O_2 conditions
27 is directly driven by lower O_2 concentrations in surface sediments and in the water column resulting in
28 higher benthic Fe fluxes and slower oxidation rates in the water column, or by a longer residence time
29 of the water mass on the shelf. However, increased benthic fluxes are in accordance with previous
30 findings from ex-situ sediment incubation experiments, where Fe fluxes increased with decreasing O_2
31 concentrations (Homoky et al., 2012). Therefore, we hypothesize that with a reduction of bottom water
32 O_2 concentrations from 50 to $30 \text{ } \mu\text{mol kg}^{-1}$, drastically more Fe is effectively released from the
33 sediments by diminished oxidation rates at the sediment-water interface, and that a large fraction gets
34 directly adsorbed onto particles. Therefore, particles do not compose a major source of Fe here, but
35 may play an important role in Fe offshore transport.



1 Due to much lower changes in concentrations of dissolved and LpCo, and the additional effect of
2 photoreduction and strong scavenging for Mn, we were unable to resolve the main mechanisms for
3 changes in Co and Mn concentrations with changes in O₂ and turbidity. Nevertheless, due to their
4 similar redox-sensitive behavior and distribution in OMZs, it is likely that they are also affected by
5 reduced O₂ conditions. The magnitude of response however, is much lower.

6 4. CONCLUSION

7 Sediments are an important source of Fe, Co and Mn to OMZ waters in the Mauritanian shelf region.
8 Remineralization and atmospheric deposition appear less important than benthic sources for dFe, with
9 vertical fluxes exceeding atmospheric fluxes but gaining importance with distance from shelf. We
10 showed that changes in O₂ concentrations from 30 to 50 μmol kg⁻¹ had a substantial influence on
11 dissolved and LpFe concentrations and to a lesser extent on Co and Mn concentrations by decreasing
12 the sediment source strength. The presence of a large part of sediment-derived Fe in the leachable
13 particulate phase highlights the importance of offshore particle transport on the Fe inventory,
14 including the dissolved form by reversible scavenging. To our knowledge, this is the first field study
15 that demonstrated strong short-term variability in redox-sensitive TMs over a few days to be directly
16 linked to changes in O₂. These findings demonstrate that projected long-term changes in oceanic O₂
17 concentrations will impact biogeochemical cycles and have important implications for global TM
18 distributions and their process parameterisations in biogeochemical models. Current models do not
19 account for small changes in O₂ on TM distributions and benthic TM fluxes. Determining the
20 processes involved and quantifying the effect of O₂ will be crucial for the implementation into current
21 modeling approaches. Not all processes could be resolved in this study, including the influence of the
22 residence time of the water masses on the shelf compared to the direct influence of O₂, and it is
23 unclear whether the changes observed on a small scale are readily transferable to a global scale.
24 Therefore, we suggest further investigations on short-term variability of O₂ and particle load in the
25 Mauritanian and other dynamic OMZs including water column TM measurement in combination with
26 benthic TM fluxes and more detailed analysis of amount and types/composition of present particles.

27

28 *Data availability.* The CTD sensor and nutrient bottle data are freely available at
29 <https://doi.pangaea.de/10.1594/PANGAEA.860480> and
30 <https://doi.pangaea.de/10.1594/PANGAEA.885109> respectively. According to the SFB754 data policy
31 (<https://www.sfb754.de/de/data>, all remaining data (trace metal data set) associated with this
32 manuscript will be published at PANGAEA (www.pangaea.de, search projects:sfb754) upon publication
33 of this manuscript.

34 *Author contributions.* IR analyzed the trace metal concentrations and drafted the manuscript. EPA and
35 MG designed the project and CS carried out the trace metal sampling at sea. J-LMB oversaw, and BW



1 carried out, the aluminium sample analysis. MD carried out the microstructure measurements at sea,
2 oversaw the calculation of the vertical flux estimates and contributed to the writing of the manuscript.
3 JL carried out the processing of microstructure data and calculation of the eddy diffusivity. JS, BG and
4 PR carried out the radium isotope analysis and their interpretation. IR and MG oversaw, and FW
5 carried out, the iodide analysis. All co-authors commented on the manuscript.

6 *Competing interests.* The authors declare that they have no conflict of interest.

7 *Acknowledgements.* The authors would like to thank the captain and the crew from RV Meteor and
8 chief scientist Dr. Stefan Sommer from the M107 cruise. This work was funded by the Deutsche
9 Forschungsgemeinschaft as part of Sonderforschungsbereich (SFB) 754: 'Climate-Biogeochemistry
10 Interactions in the Tropical Ocean'. Fabian Wolf is thanked for carrying out the analysis of iodide and
11 Peter Streu for help with the general lab work.

12 REFERENCES

- 13 Abadie, C., Lacan, F., Radic, A., Pradoux, C., and Poitrasson, F.: Iron isotopes reveal distinct
14 dissolved iron sources and pathways in the intermediate versus deep Southern Ocean, *P Natl*
15 *Acad Sci USA*, 114, 858-863, <https://doi.org/10.1073/pnas.1603107114>, 2017.
- 16 Achterberg, E. P., Steigenberger, S., Marsay, C. M., LeMoigne, F. A. C., Painter, S. C., Baker, A. R.,
17 Connelly, D. P., Moore, C. M., Tagliabue, A., and Tanhua, T.: Iron Biogeochemistry in the
18 High Latitude North Atlantic Ocean, *Sci Rep*, 8, <https://doi.org/10.1038/s41598-018-19472-1>,
19 2018.
- 20 Baker, A. R., Jickells, T. D., Witt, M., and Linge, K. L.: Trends in the solubility of iron, aluminium,
21 manganese and phosphorus in aerosol collected over the Atlantic Ocean, *Mar Chem*, 98, 43-
22 58, <https://doi.org/10.1016/j.marchem.2005.06.004>, 2006.
- 23 Baker, A. R., Adams, C., Bell, T. G., Jickells, T. D., and Ganzeveld, L.: Estimation of atmospheric
24 nutrient inputs to the Atlantic Ocean from 50°N to 50°S based on large-scale field sampling:
25 Iron and other dust-associated elements, *Global Biogeochem Cy*, 27, 755-767,
26 <https://doi.org/10.1002/gbc.20062>, 2013.
- 27 Barton, E. D.: The Poleward Undercurrent On The Eastern Boundary Of The Subtropical North
28 Atlantic. In: *Poleward Flows Along Eastern Ocean Boundaries*, Neshyba, S. J., Mooers, C. N.
29 K., Smith, R. L., and Barber, R. T. (Eds.), Springer-Verlag, New York,
30 <https://doi.org/10.1029/CE034p0082>, 1989.
- 31 Barton, E. D., Aristegui, J., Tett, P., Canton, M., Garcia-Braun, J., Hernandez-Leon, S., Nykjaer, L.,
32 Almeida, C., Almunia, J., Ballesteros, S., Basterretxea, G., Escanez, J., Garcia-Weill, L.,
33 Hernandez-Guerra, A., Lopez-Laatzén, F., Molina, R., Montero, M. F., Navarro-Perez, E.,
34 Rodriguez, J. M., van Lenning, K., Velez, H., and Wild, K.: The transition zone of the Canary



- 1 Current upwelling region, *Prog Oceanogr*, 41, 455-504, [https://doi.org/10.1016/S0079-6611\(98\)00023-8](https://doi.org/10.1016/S0079-6611(98)00023-8), 1998.
- 2
- 3 Beck, A. J., Tsukamoto, Y., Tovar-Sanchez, A., Huerta-Diaz, M., Bokuniewicz, H. J., and Sanudo-
4 Wilhelmy, S. A.: Importance of geochemical transformations in determining submarine
5 groundwater discharge-derived trace metal and nutrient fluxes, *Appl Geochem*, 22, 477-490,
6 <https://doi.org/10.1016/j.apgeochem.2006.10.005>, 2007.
- 7 Biller, D. V. and Bruland, K. W.: Sources and distributions of Mn, Fe, Co, Ni, Cu, Zn, and Cd relative
8 to macronutrients along the central California coast during the spring and summer upwelling
9 season, *Mar Chem*, 155, 50-70, <https://doi.org/10.1016/j.marchem.2013.06.003>, 2013.
- 10 Boyd, P. W.: Biogeochemistry - Iron findings, *Nature*, 446, 989-991, <https://doi.org/10.1038/446989a>, 2007.
- 11
- 12 Boyle, E. A., Lee, J.-M., Echegoyen, Y., Noble, A., Moos, S., Carrasco, G., Zhao, N., Kayser, R.,
13 Zhang, J., and Gamo, T.: Anthropogenic lead emissions in the ocean: The evolving global
14 experiment, *Oceanography*, 27, 69-75, <https://doi.org/10.5670/oceanog.2014.10>, 2014.
- 15 Brandt, P., Bange, H. W., Banyte, D., Dengler, M., Didwischus, S. H., Fischer, T., Greatbatch, R. J.,
16 Hahn, J., Kanzow, T., Karstensen, J., Krortzinger, A., Krahnmann, G., Schmidtke, S., Stramma,
17 L., Tanhua, T., and Visbeck, M.: On the role of circulation and mixing in the ventilation of
18 oxygen minimum zones with a focus on the eastern tropical North Atlantic, *Biogeosciences*,
19 12, 489-512, <https://doi.org/10.5194/bg-12-489-2015>, 2015.
- 20 Bridgestock, L., van de Flierdt, T. V., Rehkamper, M., Paul, M., Middag, R., Milne, A., Lohan, M. C.,
21 Baker, A. R., Chance, R., Khondoker, R., Strekopytov, S., Humphreys-Williams, E.,
22 Achterberg, E. P., Rijkenberg, M. J. A., Gerringa, L. J. A., and de Baar, H. J. W.: Return of
23 naturally sourced Pb to Atlantic surface waters, *Nat Commun*, 7, 12921,
24 <https://doi.org/10.1038/ncomms12921>, 2016.
- 25 Browning, T. J., Achterberg, E. P., Rapp, I., Engel, A., Bertrand, E. M., Tagliabue, A., and Moore, C.
26 M.: Nutrient co-limitation at the boundary of an oceanic gyre, *Nature*, 551, 242-246,
27 <https://doi.org/10.1038/nature24063>, 2017.
- 28 Bruland, K. W. and Lohan, M. C.: Controls of Trace Metals in Seawater. In: *The Oceans and Marine*
29 *Geochemistry*, Elderfield, H. (Ed.), *Treatise on Geochemistry*, 6, Elsevier, Oxford, 2006.
- 30 Buck, C. S., Landing, W. M., Resing, J. A., and Measures, C. I.: The solubility and deposition of
31 aerosol Fe and other trace elements in the North Atlantic Ocean: Observations from the A16N
32 CLIVAR/CO₂ repeat hydrography section, *Mar Chem*, 120, 57-70,
33 <https://doi.org/10.1016/j.marchem.2008.08.003>, 2010.
- 34 Burdige, D. J.: The biogeochemistry of manganese and iron reduction in marine sediments, *Earth-Sci*
35 *Rev*, 35, 249-284, [https://doi.org/10.1016/0012-8252\(93\)90040-E](https://doi.org/10.1016/0012-8252(93)90040-E), 1993.



- 1 Chaillou, G., Anschutz, P., Lavaux, G., Schafer, J., and Blanc, G.: The distribution of Mo, U, and Cd
2 in relation to major redox species in muddy sediments of the Bay of Biscay, *Mar Chem*, 80,
3 41-59, [https://doi.org/10.1016/S0304-4203\(02\)00097-X](https://doi.org/10.1016/S0304-4203(02)00097-X), 2002.
- 4 Charette, M. A., Morris, P. J., Henderson, P. B., and Moore, W. S.: Radium isotope distributions
5 during the US GEOTRACES North Atlantic cruises, *Mar Chem*, 177, 184-195,
6 <https://doi.org/10.1016/j.marchem.2015.01.001>, 2015.
- 7 Conway, T. M. and John, S. G.: Quantification of dissolved iron sources to the North Atlantic Ocean,
8 *Nature*, 511, 212-215, <https://doi.org/10.1038/nature13482>, 2014.
- 9 Cyr, F., Bourgault, D., Galbraith, P. S., and Gosselin, M.: Turbulent nitrate fluxes in the Lower St.
10 Lawrence Estuary, Canada, *J Geophys Res-Oceans*, 120, 2308-2330,
11 <https://doi.org/10.1002/2014jc010272>, 2015.
- 12 Dammshäuser, A., Wagener, T., and Croot, P. L.: Surface water dissolved aluminum and titanium:
13 Tracers for specific time scales of dust deposition to the Atlantic?, *Geophys Res Lett*, 38,
14 L24601, <https://doi.org/10.1029/2011gl049847>, 2011.
- 15 Elrod, V. A., Berelson, W. M., Coale, K. H., and Johnson, K. S.: The flux of iron from continental
16 shelf sediments: A missing source for global budgets, *Geophys Res Lett*, 31, L12307,
17 <https://doi.org/10.1029/2004gl020216>, 2004.
- 18 Eriksen, C. C.: Observations of internal wave reflection off sloping bottoms, *J Geophys Res-Oceans*,
19 87, 525-538, <https://doi.org/10.1029/JC087iC01p00525>, 1982.
- 20 Fitzsimmons, J. N., Zhang, R. F., and Boyle, E. A.: Dissolved iron in the tropical North Atlantic
21 Ocean, *Mar Chem*, 154, 87-99, <https://doi.org/10.1016/j.marchem.2013.05.009>, 2013.
- 22 Fitzsimmons, J. N., John, S. G., Marsay, C. M., Hoffman, C. L., Nicholas, S. L., Toner, B. M.,
23 German, C. R., and Sherrell, R. M.: Iron persistence in a distal hydrothermal plume supported
24 by dissolved-particulate exchange, *Nat Geosci*, 10, 195-201,
25 <https://doi.org/10.1038/Ngeo2900>, 2017.
- 26 Froelich, P. N., Klinkhammer, G. P., Bender, M. L., Luedtke, N. A., Heath, G. R., Cullen, D.,
27 Dauphin, P., Hammond, D., Hartman, B., and Maynard, V.: Early oxidation of organic matter
28 in pelagic sediments of the Eastern Equatorial Atlantic: suboxic diagenesis, *Geochim
29 Cosmochim Ac*, 43, 1075-1090, [https://doi.org/10.1016/0016-7037\(79\)90095-4](https://doi.org/10.1016/0016-7037(79)90095-4), 1979.
- 30 Garcia-Solsona, E., Garcia-Orellana, J., Masqué, P., and Dulaiova, H.: Uncertainties associated with
31 ^{223}Ra and ^{224}Ra measurements in water via a Delayed Coincidence Counter (RaDeCC), *Mar
32 Chem*, 109, 198-219, <https://doi.org/10.1016/j.marchem.2007.11.006>, 2008.
- 33 Gehlen, M., Beck, L., Calas, G., Flank, A. M., Van Bennekom, A. J., and Van Beusekom, J. E. E.:
34 Unraveling the atomic structure of biogenic silica: Evidence of the structural association of Al
35 and Si in diatom frustules, *Geochim Cosmochim Ac*, 66, 1601-1609,
36 [https://doi.org/10.1016/S0016-7037\(01\)00877-8](https://doi.org/10.1016/S0016-7037(01)00877-8), 2002.
- 37 Gill, A.: *Atmosphere-Ocean Dynamics*, Academic Press, California, 1982.



- 1 Grasshoff, K., Ehrhardt, M., and Kremling, K.: Methods of Seawater Analysis, Verlag Chemie,
2 Weinheim, 1983.
- 3 Green, M. A., Aller, R. C., Cochran, J. K., Lee, C., and Aller, J. Y.: Bioturbation in shelf/slope
4 sediments off Cape Hatteras, North Carolina: the use of ^{234}Th , Chl-*a*, and Br^- to evaluate rates
5 of particle and solute transport, *Deep-Sea Res Pt II*, 49, 4627-4644,
6 [https://doi.org/10.1016/S0967-0645\(02\)00132-7](https://doi.org/10.1016/S0967-0645(02)00132-7), 2002.
- 7 Hahn, J., Brandt, P., Schmidtko, S., and Krahnemann, G.: Decadal oxygen change in the eastern tropical
8 North Atlantic, *Ocean Sci*, 13, 551-576, <https://doi.org/10.5194/os-13-551-2017>, 2017.
- 9 Hansen, H. P.: Determination of oxygen, *Methods of Seawater Analysis*, Third Edition, 2007. 75-89,
10 2007.
- 11 Hatta, M., Measures, C. I., Wu, J. F., Roshan, S., Fitzsimmons, J. N., Sedwick, P., and Morton, P.: An
12 overview of dissolved Fe and Mn distributions during the 2010-2011 US GEOTRACES north
13 Atlantic cruises: GEOTRACES GA03, *Deep-Sea Res Pt II*, 116, 117-129,
14 <https://doi.org/10.1016/j.dsr2.2014.07.005>, 2015.
- 15 Hawco, N. J., Ohnemus, D. C., Resing, J. A., Twining, B. S., and Saito, M. A.: A dissolved cobalt
16 plume in the oxygen minimum zone of the eastern tropical South Pacific, *Biogeosciences*, 13,
17 5697-5717, <https://doi.org/10.5194/bg-13-5697-2016>, 2016.
- 18 Heggie, D. T.: Copper in Surface Waters of the Bering Sea, *Geochim Cosmochim Acta*, 46, 1301-1306,
19 [https://doi.org/10.1016/0016-7037\(82\)90014-X](https://doi.org/10.1016/0016-7037(82)90014-X), 1982.
- 20 Helly, J. J. and Levin, L. A.: Global distribution of naturally occurring marine hypoxia on continental
21 margins, *Deep-Sea Res Pt I*, 51, 1159-1168, <https://doi.org/10.1016/j.dsr.2004.03.009>, 2004.
- 22 Henderson, P., Morris, P., Moore, W., and Charette, M.: Methodological advances for measuring low-
23 level radium isotopes in seawater, *J Radioanal Nucl Ch*, 296, 357-362,
24 <https://doi.org/10.1007/s10967-012-2047-9>, 2013.
- 25 Homoky, W. B., Severmann, S., McManus, J., Berelson, W. M., Riedel, T. E., Statham, P. J., and
26 Mills, R. A.: Dissolved oxygen and suspended particles regulate the benthic flux of iron from
27 continental margins, *Mar Chem*, 134, 59-70, <https://doi.org/10.1016/j.marchem.2012.03.003>,
28 2012.
- 29 Homoky, W. B., Weber, T., Berelson, W. M., Conway, T. M., Henderson, G. M., van Hulten, M.,
30 Jeandel, C., Severmann, S., and Tagliabue, A.: Quantifying trace element and isotope fluxes at
31 the ocean-sediment boundary: a review, *Philos T R Soc A*, 374, 20160246,
32 <https://doi.org/10.1098/rsta.2016.0246>, 2016.
- 33 Hurst, M. P., Aguilar-Islas, A. M., and Bruland, K. W.: Iron in the southeastern Bering Sea: Elevated
34 leachable particulate Fe in shelf bottom waters as an important source for surface waters, *Cont
35 Shelf Res*, 30, 467-480, <https://doi.org/10.1016/j.csr.2010.01.001>, 2010.



- 1 Hydes, D. J. and Liss, P. S.: Fluorimetric method for determination of low concentrations of dissolved
2 aluminum in natural waters, *Analyst*, 101, 922-931, <https://doi.org/10.1039/an9760100922>,
3 1976.
- 4 John, S. G. and Adkins, J.: The vertical distribution of iron stable isotopes in the North Atlantic near
5 Bermuda, *Global Biogeochem Cy*, 26, GB2034, <https://doi.org/10.1029/2011gb004043>, 2012.
- 6 Johnson, K. S., Stout, P. M., Berelson, W. M., and Sakamotoarnold, C. M.: Cobalt and copper
7 distributions in the waters of Santa-Monica Basin, California, *Nature*, 332, 527-530,
8 <https://doi.org/10.1038/332527a0>, 1988.
- 9 Kagaya, S., Maeba, E., Inoue, Y., Kamichatani, W., Kajiwara, T., Yanai, H., Saito, M., and Tohda, K.:
10 A solid phase extraction using a chelate resin immobilizing carboxymethylated
11 pentaethylenehexamine for separation and preconcentration of trace elements in water
12 samples, *Talanta*, 79, 146-152, <https://doi.org/10.1016/j.talanta.2009.03.016>, 2009.
- 13 Karstensen, J., Stramma, L., and Visbeck, M.: Oxygen minimum zones in the eastern tropical Atlantic
14 and Pacific oceans, *Prog Oceanogr*, 77, 331-350,
15 <https://doi.org/10.1016/j.pocean.2007.05.009>, 2008.
- 16 Klenz, T., Dengler, M., and Brandt, P.: Seasonal variability of the Mauritanian Undercurrent and
17 Hydrography at 18°N, *J Geophys Res: Oceans*, in press,
18 <https://doi.org/10.1029/2018JC014264>, 2018.
- 19 Köllner, M., Visbeck, M., Tanhua, T., and Fischer, T.: Diapycnal diffusivity in the core and oxycline
20 of the tropical North Atlantic oxygen minimum zone, *J Marine Syst*, 160, 54-63,
21 <https://doi.org/10.1016/j.jmarsys.2016.03.012>, 2016.
- 22 Labatut, M., Lacan, F., Pradoux, C., Chmeleff, J., Radic, A., Murray, J. W., Poitrasson, F., Johansen,
23 A. M., and Thil, F.: Iron sources and dissolved-particulate interactions in the seawater of the
24 Western Equatorial Pacific, iron isotope perspectives, *Global Biogeochem Cy*, 28, 1044-1065,
25 <https://doi.org/10.1002/2014gb004928>, 2014.
- 26 Lam, P. J. and Bishop, J. K. B.: The continental margin is a key source of iron to the HNLC North
27 Pacific Ocean, *Geophys Res Lett*, 35, L07608, <https://doi.org/10.1029/2008gl033294>, 2008.
- 28 Lam, P. J., Ohnemus, D. C., and Marcus, M. A.: The speciation of marine particulate iron adjacent to
29 active and passive continental margins, *Geochim Cosmochim Ac*, 80, 108-124,
30 <https://doi.org/10.1016/j.gca.2011.11.044>, 2012.
- 31 Liu, X. W. and Millero, F. J.: The solubility of iron in seawater, *Mar Chem*, 77, 43-54,
32 [https://doi.org/10.1016/S0304-4203\(01\)00074-3](https://doi.org/10.1016/S0304-4203(01)00074-3), 2002.
- 33 Lohan, M. C. and Bruland, K. W.: Elevated Fe(II) and dissolved Fe in hypoxic shelf waters off
34 Oregon and Washington: An enhanced source of iron to coastal upwelling regimes, *Environ*
35 *Sci Technol*, 42, 6462-6468, <https://doi.org/10.1021/es800144j>, 2008.



- 1 Luther, G. W., Swartz, C. B., and Ullman, W. J.: Direct determination of iodide in seawater by
2 Cathodic Stripping Square-Wave Voltammetry, *Anal Chem*, 60, 1721-1724,
3 <https://doi.org/10.1021/ac00168a017>, 1988.
- 4 Mahowald, N. M., Engelstaedter, S., Luo, C., Sealy, A., Artaxo, P., Benitez-Nelson, C., Bonnet, S.,
5 Chen, Y., Chuang, P. Y., Cohen, D. D., Dulac, F., Herut, B., Johansen, A. M., Kubilay, N.,
6 Losno, R., Maenhaut, W., Paytan, A., Prospero, J. A., Shank, L. M., and Siefert, R. L.:
7 Atmospheric Iron Deposition: Global Distribution, Variability, and Human Perturbations,
8 *Annu Rev Mar Sci*, 1, 245-278, <https://doi.org/10.1146/annurev.marine.010908.163727>, 2009.
- 9 Martin, J. H., Gordon, R. M., Fitzwater, S., and Broenkow, W. W.: Vertex - Phytoplankton Iron
10 Studies in the Gulf of Alaska, *Deep-Sea Res*, 36, 649-680, [https://doi.org/10.1016/0198-](https://doi.org/10.1016/0198-0149(89)90144-1)
11 [0149\(89\)90144-1](https://doi.org/10.1016/0198-0149(89)90144-1), 1989.
- 12 Mawji, E. and Schlitzer, R. and Dodas, E. M. and Abadie, C. and Abouchami, W. and Anderson, R. F.
13 and Baars, O. and Bakker, K. and Baskaran, M. and Bates, N. R. and Bluhm, K. and Bowie,
14 A. and Bown, J. and Boye, M. and Boyle, E. A. and Branellec, P. and Bruland, K. W. and
15 Brzezinski, M. A. and Bucciarelli, E. and Buesseler, K. and Butler, E. and Cai, P. H. and
16 Cardinal, D. and Casciotti, K. and Chaves, J. and Cheng, H. and Chever, F. and Church, T. M.
17 and Colman, A. S. and Conway, T. M. and Croot, P. L. and Cutter, G. A. and de Baar, H. J.
18 W. and de Souza, G. F. and Dehairs, F. and Deng, F. F. and Dieu, H. T. and Dulaquais, G. and
19 Echevoyen-Sanz, Y. and Edwards, R. L. and Fahrbach, E. and Fitzsimmons, J. and Fleisher,
20 M. and Frank, M. and Friedrich, J. and Fripiat, F. and Galer, S. J. G. and Gamo, T. and
21 Solsona, E. G. and Gerringa, L. J. A. and Godoy, J. M. and Gonzalez, S. and Grosstefan, E.
22 and Hatta, M. and Hayes, C. T. and Heller, M. I. and Henderson, G. and Huang, K. F. and
23 Jeandel, C. and Jenkins, W. J. and John, S. and Kenna, T. C. and Klunder, M. and Kretschmer,
24 S. and Kumamoto, Y. and Laan, P. and Labatut, M. and Lacan, F. and Lam, P. J. and
25 Lannuzel, D. and le Moigne, F. and Lechtenfeld, O. J. and Lohan, M. C. and Lu, Y. B. and
26 Masque, P. and McClain, C. R. and Measures, C. and Middag, R. and Moffett, J. and Navidad,
27 A. and Nishioka, J. and Noble, A. and Obata, H. and Ohnemus, D. C. and Owens, S. and
28 Planchon, F. and Pradoux, C. and Puigcorbe, V. and Quay, P. and Radic, A. and Rehkamper,
29 M. and Remenyi, T. and Rijkenberg, M. J. A. and Rintoul, S. and Robinson, L. F. and Roeske,
30 T. and Rosenberg, M. and van der Loeff, M. R. and Ryabenko, E. and Saito, M. A. and
31 Roshan, S. and Salt, L. and Sarthou, G. and Schauer, U. and Scott, P. and Sedwick, P. N. and
32 Sha, L. J. and Shiller, A. M. and Sigman, D. M. and Smethie, W. and Smith, G. J. and Sohrin,
33 Y. and Speich, S. and Stichel, T. and Stutsman, J. and Swift, J. H. and Tagliabue, A. and
34 Thomas, A. and Tsunogai, U. and Twining, B. S. and van Aken, H. M. and van Heuven, S.
35 and van Ooijen, J. and van Weerlee, E. and Venchiarutti, C. and Voelker, A. H. L. and Wake,
36 B. and Warner, M. J. and Woodward, E. M. S. and Wu, J. F. and Wyatt, N. and Yoshikawa, H.
37 and Zheng, X. Y. and Xue, Z. C. and Zieringer, M. and Zimmer, L. A.: The GEOTRACES



- 1 Intermediate Data Product 2014, Mar Chem, 177, 1-8,
2 <https://doi.org/10.1016/j.marchem.2015.04.005>, 2015.
- 3 McLennan, S. M.: Relationships between the trace element composition of sedimentary rocks and
4 upper continental crust, *Geochem Geophys Geosy*, 2, 1021,
5 <https://doi.org/10.1029/2000GC000109>, 2001.
- 6 Measures, C. I. and Brown, E. T.: Estimating dust input to the Atlantic Ocean using surface water
7 aluminium concentrations. In: *The impact of desert dust across the Mediterranean*, Guerzoni,
8 S. and Chester, R. (Eds.), Environmental Science and Technology Library, Springer,
9 Dordrecht, 1996.
- 10 Measures, C. I. and Vink, S.: On the use of dissolved aluminum in surface waters to estimate dust
11 deposition to the ocean, *Global Biogeochem Cy*, 14, 317-327,
12 <https://doi.org/10.1029/1999gb001188>, 2000.
- 13 Menzel Barraqueta, J.-L., Schlosser, C., Planquette, H., Gourain, A., Cheize, M., Boutorh, J., Shelley,
14 R., Pereira, L. C., Gledhill, M., Hopwood, M. J., Lacan, F., Lherminier, P., Sarthou, G., and
15 Achterberg, E. P.: Aluminium in the North Atlantic Ocean and the Labrador Sea
16 (GEOTRACES GA01 section): roles of continental inputs and biogenic particle removal,
17 *Biogeosciences*, 15, 5271-5286, <https://doi.org/10.5194/bg-15-5271-2018>, 2018.
- 18 Middag, R., de Baar, H. J. W., Laan, P., and Huhn, O.: The effects of continental margins and water
19 mass circulation on the distribution of dissolved aluminum and manganese in Drake Passage, *J*
20 *Geophys Res-Oceans*, 117, C01019, <https://doi.org/10.1029/2011jc007434>, 2012.
- 21 Milne, A., Schlosser, C., Wake, B. D., Achterberg, E. P., Chance, R., Baker, A. R., Forryan, A., and
22 Lohan, M. C.: Particulate phases are key in controlling dissolved iron concentrations in the
23 (sub)tropical North Atlantic, *Geophys Res Lett*, 44, 2377-2387,
24 <https://doi.org/10.1002/2016gl072314>, 2017.
- 25 Mittelstaedt, E.: The upwelling area off Northwest Africa—A description of phenomena related to
26 coastal upwelling, *Prog Oceanogr*, 12, 307-331, [https://doi.org/10.1016/0079-6611\(83\)90012-](https://doi.org/10.1016/0079-6611(83)90012-5)
27 5, 1983.
- 28 Mittelstaedt, E.: The ocean boundary along the northwest African coast: Circulation and
29 oceanographic properties at the sea-surface, *Prog Oceanogr*, 26, 307-355,
30 [https://doi.org/10.1016/0079-6611\(91\)90011-A](https://doi.org/10.1016/0079-6611(91)90011-A), 1991.
- 31 Moffett, J. W.: The Relationship between cerium and manganese oxidation in the marine environment,
32 *Limnol Oceanogr*, 39, 1309-1318, <https://doi.org/10.4319/lo.1994.39.6.1309>, 1994.
- 33 Moffett, J. W. and Ho, J.: Oxidation of cobalt and manganese in seawater via a common microbially
34 catalyzed pathway, *Geochim Cosmochim Acta*, 60, 3415-3424, [https://doi.org/10.1016/0016-](https://doi.org/10.1016/0016-7037(96)00176-7)
35 7037(96)00176-7, 1996.
- 36 Moffett, J. W. and Zika, R. G.: Reaction kinetics of hydrogen peroxide with copper and iron in
37 seawater, *Environ Sci Technol*, 21, 804-810, <https://doi.org/10.1021/es00162a012>, 1987.



- 1 Moffett, J. W., Vedamati, J., Goepfert, T. J., Pratihary, A., Gauns, M., and Naqvi, S. W. A.:
2 Biogeochemistry of iron in the Arabian Sea, *Limnol Oceanogr*, 60, 1671-1688,
3 <https://doi.org/10.1002/lno.10132>, 2015.
- 4 Moore, C. M., Mills, M. M., Achterberg, E. P., Geider, R. J., LaRoche, J., Lucas, M. I., McDonagh, E.
5 L., Pan, X., Poulton, A. J., Rijkenberg, M. J. A., Suggett, D. J., Ussher, S. J., and Woodward,
6 E. M. S.: Large-scale distribution of Atlantic nitrogen fixation controlled by iron availability,
7 *Nat Geosci*, 2, 867-871, <https://doi.org/10.1038/ngeo667>, 2009.
- 8 Moore, C. M., Mills, M. M., Arrigo, K. R., Berman-Frank, I., Bopp, L., Boyd, P. W., Galbraith, E. D.,
9 Geider, R. J., Guieu, C., Jaccard, S. L., Jickells, T. D., La Roche, J., Lenton, T. M., Mahowald,
10 N. M., Maranon, E., Marinov, I., Moore, J. K., Nakatsuka, T., Oschlies, A., Saito, M. A.,
11 Thingstad, T. F., Tsuda, A., and Ulloa, O.: Processes and patterns of oceanic nutrient
12 limitation, *Nat Geosci*, 6, 701-710, <https://doi.org/10.1038/Ngeo1765>, 2013.
- 13 Moore, W. S.: ^{228}Ra in the South-Atlantic Bight, *J Geophys Res-Oceans*, 92, 5177-5190,
14 <https://doi.org/10.1029/JC092iC05p05177>, 1987.
- 15 Moore, W. S.: Ages of continental shelf waters determined from ^{223}Ra and ^{224}Ra , *J Geophys Res-*
16 *Oceans*, 105, 22117-22122, <https://doi.org/10.1029/1999jc000289>, 2000.
- 17 Moore, W. S.: Seasonal distribution and flux of radium isotopes on the southeastern U.S. continental
18 shelf, *J Geophys Res*, 112, C10013, <https://doi.org/10.1029/2007JC004199>, 2007.
- 19 Moore, W. S. and Arnold, R.: Measurement of ^{223}Ra and ^{224}Ra in coastal waters using a delayed
20 coincidence counter, *J Geophys Res*, 101, 1321-1329, <https://doi.org/10.1029/95jc03139>,
21 1996.
- 22 Moore, W. S. and Cai, P.: Calibration of RaDeCC systems for ^{223}Ra measurements, *Mar Chem*, 156,
23 130-137, <https://doi.org/10.1016/j.marchem.2013.03.002>, 2013.
- 24 Moran, S. B. and Moore, R. M.: The potential source of dissolved aluminum from resuspended
25 sediments to the North Atlantic Deep Water, *Geochim Cosmochim Acta*, 55, 2745-2751,
26 [https://doi.org/10.1016/0016-7037\(91\)90441-7](https://doi.org/10.1016/0016-7037(91)90441-7), 1991.
- 27 Morel, F. M. M. and Price, N. M.: The biogeochemical cycles of trace metals in the oceans, *Science*,
28 300, 944-947, <https://doi.org/10.1126/science.1083545>, 2003.
- 29 Naykki, T., Virtanen, A., Kaukonen, L., Magnusson, B., Vaisanen, T., and Leito, I.: Application of the
30 Nordtest method for "real-time" uncertainty estimation of on-line field measurement, *Environ*
31 *Monit Assess*, 187, 360, <https://doi.org/10.1007/s10661-015-4856-0>, 2015.
- 32 Noble, A. E., Lamborg, C. H., Ohnemus, D. C., Lam, P. J., Goepfert, T. J., Measures, C. I., Frame, C.
33 H., Casciotti, K. L., DiTullio, G. R., Jennings, J., and Saito, M. A.: Basin-scale inputs of
34 cobalt, iron, and manganese from the Benguela-Angola front to the South Atlantic Ocean,
35 *Limnol Oceanogr*, 57, 989-1010, <https://doi.org/10.4319/lo.2012.57.4.0989>, 2012.
- 36 Noble, A. E., Echegoyen-Sanz, Y., Boyle, E. A., Ohnemus, D. C., Lam, P. J., Kayser, R., Reuer, M.,
37 Wu, J. F., and Smethie, W.: Dynamic variability of dissolved Pb and Pb isotope composition



- 1 from the US North Atlantic GEOTRACES transect, *Deep-Sea Res Pt II*, 116, 208-225,
2 <https://doi.org/10.1016/j.dsr2.2014.11.011>, 2015.
- 3 Noble, A. E., Ohnemus, D. C., Hawco, N. J., Lam, P. J., and Saito, M. A.: Coastal sources, sinks and
4 strong organic complexation of dissolved cobalt within the US North Atlantic GEOTRACES
5 transect GA03, *Biogeosciences*, 14, 2715-2739, <https://doi.org/10.5194/bg-14-2715-2017>,
6 2017.
- 7 Noffke, A., Hensen, C., Sommer, S., Scholz, F., Bohlen, L., Mosch, T., Graco, M., and Wallmann, K.:
8 Benthic iron and phosphorus fluxes across the Peruvian oxygen minimum zone, *Limnol*
9 *Oceanogr*, 57, 851-867, <https://doi.org/10.4319/lo.2012.57.3.0851>, 2012.
- 10 Nriagu, J. O. and Pacyna, J. M.: Quantitative assessment of worldwide contamination of air, water and
11 soils by trace metals, *Nature*, 333, 134-139, <https://doi.org/10.1038/333134a0>, 1988.
- 12 Nychka, D., Furrer, R., Paige, J., and Sain, S.: fields: Tools for Spatial Data, R package version 8.3-6,
13 <https://CRAN.R-project.org/package=fields>, 2016.
- 14 Oksanen, J., Blanchet, F. G., Friendly, M., Kindt, R., Legendre, P., McGlinn, D., Minchin, P., B.
15 O'Hara, R., Simpson, G., Solymos, P., Stevens, H., Szöcs, E., and Wagner, H.: vegan:
16 Community Ecology Package. Ordination methods, diversity analysis and other functions for
17 community and vegetation ecologists, version 2.4-4, [https://CRAN.R-](https://CRAN.R-project.org/package=vegan)
18 [project.org/package=vegan](https://CRAN.R-project.org/package=vegan), 2017.
- 19 Oldham, V. E., Jones, M. R., Tebo, B. M., and Luther, G. W.: Oxidative and reductive processes
20 contributing to manganese cycling at oxic-anoxic interfaces, *Mar Chem*, 195, 122-128,
21 <https://doi.org/10.1016/j.marchem.2017.06.002>, 2017.
- 22 Orians, K. J. and Bruland, K. W.: Dissolved aluminum in the Central North Pacific, *Nature*, 316, 427-
23 429, <https://doi.org/10.1038/316427a0>, 1985.
- 24 Orians, K. J. and Bruland, K. W.: The biogeochemistry of aluminum in the Pacific Ocean, *Earth*
25 *Planet Sc Lett*, 78, 397-410, [https://doi.org/10.1016/0012-821x\(86\)90006-3](https://doi.org/10.1016/0012-821x(86)90006-3), 1986.
- 26 Osborn, T. R.: Estimates of the local rate of vertical diffusion from dissipation measurements, *J Phys*
27 *Oceanogr*, 10, 83-89, [https://doi.org/10.1175/1520-0485\(1980\)010<0083:Eotlro>2.0.Co;2](https://doi.org/10.1175/1520-0485(1980)010<0083:Eotlro>2.0.Co;2),
28 1980.
- 29 Parker, D. L., Morita, T., Mozafarzadeh, M. L., Verity, R., McCarthy, J. K., and Tebo, B. M.: Inter-
30 relationships of MnO₂ precipitation, siderophore-Mn(III) complex formation, siderophore
31 degradation, and iron limitation in Mn(II)-oxidizing bacterial cultures, *Geochim Cosmochim*
32 *Ac*, 71, 5672-5683, <https://doi.org/10.1016/j.gca.2007.03.042>, 2007.
- 33 Patey, M. D., Achterberg, E. P., Rijkenberg, M. J., and Pearce, R.: Aerosol time-series measurements
34 over the tropical Northeast Atlantic Ocean: Dust sources, elemental composition and
35 mineralogy, *Mar Chem*, 174, 103-119, <https://doi.org/10.1016/j.marchem.2015.06.004>, 2015.



- 1 Peña-Izquierdo, J., van Sebille, E., Pelegri, J. L., Sprintall, J., Mason, E., Llanillo, P. J., and Machin,
2 F.: Water mass pathways to the North Atlantic oxygen minimum zone, *J Geophys Res-*
3 *Oceans*, 120, 3350-3372, <https://doi.org/10.1002/2014jc010557>, 2015.
- 4 Rama and Moore, W. S.: Using the radium quartet for evaluating groundwater input and water
5 exchange in salt marshes, *Geochim Cosmochim Acta*, 60, 4645-4652,
6 [https://doi.org/10.1016/S0016-7037\(96\)00289-X](https://doi.org/10.1016/S0016-7037(96)00289-X), 1996.
- 7 Rapp, I., Schlosser, C., Rusiecka, D., Gledhill, M., and Achterberg, E. P.: Automated preconcentration
8 of Fe, Zn, Cu, Ni, Cd, Pb, Co, and Mn in seawater with analysis using high-resolution sector
9 field inductively-coupled plasma mass spectrometry, *Anal Chim Acta*, 976, 1-13,
10 <https://doi.org/10.1016/j.aca.2017.05.008>, 2017.
- 11 Ricciardulli, L. and Wentz, F. J.: Remote Sensing Systems ASCAT C-2015 Daily Ocean Vector
12 Winds on 0.25 deg grid, Version 02.1. Santa Rosa, CA: Remote Sensing Systems. Available at
13 www.remss.com/missions/ascats, 2016.
- 14 Rijkenberg, M. J. A., Steigenberger, S., Powell, C. F., van Haren, H., Patey, M. D., Baker, A. R., and
15 Achterberg, E. P.: Fluxes and distribution of dissolved iron in the eastern (sub-) tropical North
16 Atlantic Ocean, *Global Biogeochem Cy*, 26, GB3004, <https://doi.org/10.1029/2011gb004264>,
17 2012.
- 18 Rijkenberg, M. J. A., Middag, R., Laan, P., Gerringa, L. J. A., van Aken, H. M., Schoemann, V., de
19 Jong, J. T. M., and de Baar, H. J. W.: The distribution of dissolved iron in the West Atlantic
20 Ocean, *Plos One*, 9, e101323, <https://doi.org/10.1371/journal.pone.0101323>, 2014.
- 21 Rudnick, R. L. and Gao, S.: Composition of the continental crust. In: *Treatise on geochemistry*,
22 Holland, H. D. and Turekian, K. K. (Eds.), Pergamon, Oxford, UK, 2006.
- 23 Rue, E. L., Smith, G. J., Cutter, G. A., and Bruland, K. W.: The response of trace element redox
24 couples to suboxic conditions in the water column, *Deep-Sea Res Pt I*, 44, 113-134,
25 [https://doi.org/10.1016/S0967-0637\(96\)00088-X](https://doi.org/10.1016/S0967-0637(96)00088-X), 1997.
- 26 Rusiecka, D., Gledhill, M., Milne, A., Achterberg, E. P., Annett, A. L., Atkinson, S., Birchill, A.,
27 Karstensen, J., Lohan, M., Mariez, C., Middag, R., Rolison, J. M., Tanhua, T., Ussher, S., and
28 Connelly, D.: Anthropogenic signatures of lead in the Northeast Atlantic, *Geophys Res Lett*,
29 45, 2734-2743, <https://doi.org/10.1002/2017gl076825>, 2018.
- 30 Saito, M. A., Goepfert, T. J., and Ritt, J. T.: Some thoughts on the concept of colimitation: Three
31 definitions and the importance of bioavailability, *Limnol Oceanogr*, 53, 276-290,
32 <https://doi.org/10.4319/l0.2008.53.1.0276>, 2008.
- 33 Schafstall, J., Dengler, M., Brandt, P., and Bange, H.: Tidal-induced mixing and diapycnal nutrient
34 fluxes in the Mauritanian upwelling region, *J Geophys Res-Oceans*, 115, C10014,
35 <https://doi.org/10.1029/2009jc005940>, 2010.
- 36 Schlitzer, R. and Anderson, R. F. and Dodas, E. M. and Lohan, M. and Geibert, W. and Tagliabue, A.
37 and Bowie, A. and Jeandel, C. and Maldonado, M. T. and Landing, W. M. and Cockwell, D.



1 and Abadie, C. and Abouchami, W. and Achterberg, E. P. and Agather, A. and Aguiar-Islas,
2 A. and van Aken, H. M. and Andersen, M. and Archer, C. and Auro, M. and de Baar, H. J. and
3 Baars, O. and Baker, A. R. and Bakker, K. and Basak, C. and Baskaran, M. and Bates, N. R.
4 and Bauch, D. and van Beek, P. and Behrens, M. K. and Black, E. and Bluhm, K. and Bopp,
5 L. and Bouman, H. and Bowman, K. and Bown, J. and Boyd, P. and Boye, M. and Boyle, E.
6 A. and Branellec, P. and Bridgestock, L. and Brissebrat, G. and Browning, T. and Bruland, K.
7 W. and Brumsack, H.-J. and Brzezinski, M. and Buck, C. S. and Buck, K. N. and Buesseler,
8 K. and Bull, A. and Butler, E. and Cai, P. and Mor, P. C. and Cardinal, D. and Carlson, C. and
9 Carrasco, G. and Casacuberta, N. and Casciotti, K. L. and Castrillejo, M. and Chamizo, E. and
10 Chance, R. and Charette, M. A. and Chaves, J. E. and Cheng, H. and Chever, F. and Christl,
11 M. and Church, T. M. and Closset, I. and Colman, A. and Conway, T. M. and Cossa, D. and
12 Croot, P. and Cullen, J. T. and Cutter, G. A. and Daniels, C. and Dehairs, F. and Deng, F. and
13 Dieu, H. T. and Duggan, B. and Dulaquais, G. and Dumousseaud, C. and Echevoyen-Sanz, Y.
14 and Edwards, R. L. and Ellwood, M. and Fahrbach, E. and Fitzsimmons, J. N. and Russell
15 Flegal, A. and Fleisher, M. Q. and van de Flierdt, T. and Frank, M. and Friedrich, J. and
16 Fripiat, F. and Fröllje, H. and Galer, S. J. G. and Gamo, T. and Ganeshram, R. S. and Garcia-
17 Orellana, J. and Garcia-Solsona, E. and Gault-Ringold, M. and George, E. and Gerringa, L. J.
18 A. and Gilbert, M. and Godoy, J. M. and Goldstein, S. L. and Gonzalez, S. R. and Grissom, K.
19 and Hammerschmidt, C. and Hartman, A. and Hassler, C. S. and Hathorne, E. C. and Hatta,
20 M. and Hawco, N. and Hayes, C. T. and Heimbürger, L.-E. and Helgoe, J. and Heller, M. and
21 Henderson, G. M. and Henderson, P. B. and van Heuven, S. and Ho, P. and Horner, T. J. and
22 Hsieh, Y.-T. and Huang, K.-F. and Humphreys, M. P. and Isshiki, K. and Jacquot, J. E. and
23 Janssen, D. J. and Jenkins, W. J. and John, S. and Jones, E. M. and Jones, J. L. and Kadko, D.
24 C. and Kayser, R. and Kenna, T. C. and Khondoker, R. and Kim, T. and Kipp, L. and Klar, J.
25 K. and Klunder, M. and Kretschmer, S. and Kumamoto, Y. and Laan, P. and Labatut, M. and
26 Lacan, F. and Lam, P. J. and Lambelet, M. and Lamborg, C. H. and Le Moigne, F. A. C. and
27 Le Roy, E. and Lechtenfeld, O. J. and Lee, J.-M. and Lherminier, P. and Little, S. and López-
28 Lora, M. and Lu, Y. and Masque, P. and Mawji, E. and McClain, C. R. and Measures, C. and
29 Mehic, S. and Barraqueta, J.-L. M. and van der Merwe, P. and Middag, R. and Mieruch, S.
30 and Milne, A. and Minami, T. and Moffett, J. W. and Moncoiffe, G. and Moore, W. S. and
31 Morris, P. J. and Morton, P. L. and Nakaguchi, Y. and Nakayama, N. and Niedermiller, J. and
32 Nishioka, J. and Nishiuchi, A. and Noble, A. and Obata, H. and Ober, S. and Ohnemus, D. C.
33 and van Ooijen, J. and O'Sullivan, J. and Owens, S. and Pahnke, K. and Paul, M. and Pavia, F.
34 and Pena, L. D. and Peters, B. and Planchon, F. and Planquette, H. and Pradoux, C. and
35 Puigcorbé, V. and Quay, P. and Queroue, F. and Radic, A. and Rauschenberg, S. and
36 Rehkämper, M. and Rember, R. and Remenyi, T. and Resing, J. A. and Rickli, J. and Rigaud,
37 S. and Rijkenberg, M. J. A. and Rintoul, S. and Robinson, L. F. and Roca-Martí, M. and



- 1 Rodellas, V. and Roeske, T. and Rolison, J. M. and Rosenberg, M. and Roshan, S. and Rutgers
2 van der Loeff, M. M. and Ryabenko, E. and Saito, M. A. and Salt, L. A. and Sanial, V. and
3 Sarthou, G. and Schallenberg, C. and Schauer, U. and Scher, H. and Schlosser, C. and
4 Schnetger, B. and Scott, P. and Sedwick, P. N. and Semiletov, I. and Shelley, R. and Sherrell,
5 R. M. and Shiller, A. M. and Sigman, D. M. and Singh, S. K. and Slagter, H. A. and Slater, E.
6 and Smethie, W. M. and Snaith, H. and Sohrin, Y. and Sohst, B. and Sonke, J. E. and Speich,
7 S. and Steinfeldt, R. and Stewart, G. and Stichel, T. and Stirling, C. H. and Stutsman, J. and
8 Swarr, G. J. and Swift, J. H. and Thomas, A. and Thorne, K. and Till, C. P. and Till, R. and
9 Townsend, A. T. and Townsend, E. and Tuerena, R. and Twining, B. S. and Vance, D. and
10 Velazquez, S. and Venchiarutti, C. and Villa-Alfageme, M. and Vivancos, S. M. and Voelker,
11 A. H. L. and Wake, B. and Warner, M. J. and Watson, R. and van Weerlee, E. and Alexandra
12 Weigand, M. and Weinstein, Y. and Weiss, D. and Wisotzki, A. and Woodward, E. M. S. and
13 Wu, J. and Wu, Y. and Wuttig, K. and Wyatt, N. and Xiang, Y. and Xie, R. C. and Xue, Z. and
14 Yoshikawa, H. and Zhang, J. and Zhang, P. and Zhao, Y. and Zheng, L. and Zheng, X.-Y. and
15 Zieringer, M. and Zimmer, L. A. and Ziveri, P. and Zunino, P. and Zurbrück, C.: The
16 GEOTRACES Intermediate Data Product 2017, *Chem Geol*, 493, 210-223,
17 <https://doi.org/10.1016/j.chemgeo.2018.05.040>, 2018.
- 18 Schlosser, C., Streu, P., Frank, M., Lavik, G., Croot, P. L., Dengler, M., and Achterberg, E. P.: H₂S
19 events in the Peruvian oxygen minimum zone facilitate enhanced dissolved Fe concentrations,
20 *Sci Rep*, 8, <https://doi.org/10.1038/s41598-018-30580-w>, 2018.
- 21 Schmidtko, S., Stramma, L., and Visbeck, M.: Decline in global oceanic oxygen content during the
22 past five decades, *Nature*, 542, 335-339, <https://doi.org/10.1038/nature21399>, 2017.
- 23 Scholten, J. C., Pham, M. K., Blinova, O., Charette, M. A., Dulaiova, H., and Eriksson, M.:
24 Preparation of Mn-fiber standards for the efficiency calibration of the delayed coincidence
25 counting system (RaDeCC), *Mar Chem*, 121, 206-214,
26 <https://doi.org/10.1016/j.marchem.2010.04.009>, 2010.
- 27 Scholz, F., Loscher, C. R., Fiskal, A., Sommer, S., Hensen, C., Lomnitz, U., Wuttig, K., Gottlicher, J.,
28 Kossel, E., Steininger, R., and Canfield, D. E.: Nitrate-dependent iron oxidation limits iron
29 transport in anoxic ocean regions, *Earth Planet Sc Lett*, 454, 272-281,
30 <https://doi.org/10.1016/j.epsl.2016.09.025>, 2016.
- 31 Schroller-Lomnitz, U., Hensen, C., Dale, A. W., Scholz, F., Clemens, D., Sommer, S., Noffke, A., and
32 Wallmann, K.: Dissolved benthic phosphate, iron and carbon fluxes in the Mauritanian
33 upwelling system and implications for ongoing deoxygenation, *Deep-Sea Res Pt I*, in review,
34 2018.
- 35 Severmann, S., McManus, J., Berelson, W. M., and Hammond, D. E.: The continental shelf benthic
36 iron flux and its isotope composition, *Geochim Cosmochim Ac*, 74, 3984-4004,
37 <https://doi.org/10.1016/j.gca.2010.04.022>, 2010.



- 1 Shelley, R. U., Morton, P. L., and Landing, W. M.: Elemental ratios and enrichment factors in aerosols
2 from the US-GEOTRACES North Atlantic transects, *Deep-Sea Res Pt II*, 116, 262-272,
3 <https://doi.org/10.1016/j.dsr2.2014.12.005>, 2015.
- 4 Shelley, R. U., Landing, W. M., Ussher, S. J., Planquette, H., and Sarthou, G.: Regional trends in the
5 fractional solubility of Fe and other metals from North Atlantic aerosols (GEOTRACES
6 cruises GA01 and GA03) following a two-stage leach, *Biogeosciences*, 15, 2271-2288,
7 <https://doi.org/10.5194/bg-15-2271-2018>, 2018.
- 8 Sherrell, R. M. and Boyle, E. A.: The trace metal composition of suspended particles in the oceanic
9 water column near Bermuda, *Earth Planet Sc Lett*, 111, 155-174, [https://doi.org/10.1016/0012-821x\(92\)90176-V](https://doi.org/10.1016/0012-821x(92)90176-V), 1992.
- 11 Soataert, K., Petzoldt, T., and Meysman, F.: marelac: Tools for Aquatic Sciences, Version 2.1.6,
12 <https://CRAN.R-project.org/package=marelac>, 2016. 2016.
- 13 Steinfeldt, R., Sultenfuss, J., Dengler, M., Fischer, T., and Rhein, M.: Coastal upwelling off Peru and
14 Mauritania inferred from helium isotope disequilibrium, *Biogeosciences*, 12, 7519-7533,
15 <https://doi.org/10.5194/bg-12-7519-2015>, 2015.
- 16 Stramma, L., Brandt, P., Schafstall, J., Schott, F., Fischer, J., and Kortzinger, A.: Oxygen minimum
17 zone in the North Atlantic south and east of the Cape Verde Islands, *J Geophys Res-Oceans*,
18 113, C04014, <https://doi.org/10.1029/2007jc004369>, 2008a.
- 19 Stramma, L., Johnson, G. C., Sprintall, J., and Mohrholz, V.: Expanding oxygen-minimum zones in
20 the tropical oceans, *Science*, 320, 655-658, <https://doi.org/10.1126/science.1153847>, 2008b.
- 21 Stumm, W. and Morgan, J. J.: *Aquatic Chemistry: Chemical Equilibria and Rates in Natural Waters*,
22 John Wiley & Sons, New York, 1995.
- 23 Sunda, W. G. and Huntsman, S. A.: Effect of sunlight on redox cycles of manganese in the
24 Southwestern Sargasso Sea, *Deep-Sea Res*, 35, 1297-1317, [https://doi.org/10.1016/0198-0149\(88\)90084-2](https://doi.org/10.1016/0198-0149(88)90084-2), 1988.
- 26 Sunda, W. G. and Huntsman, S. A.: Photoreduction of manganese oxides in seawater, *Mar Chem*, 46,
27 133-152, [https://doi.org/10.1016/0304-4203\(94\)90051-5](https://doi.org/10.1016/0304-4203(94)90051-5), 1994.
- 28 Tebo, B. M. and Emerson, S.: Microbial manganese(II) oxidation in the marine environment: a
29 quantitative study, *Biogeochemistry*, 2, 149-161, <https://doi.org/10.1007/Bf02180192>, 1986.
- 30 Tebo, B. M., Bargar, J. R., Clement, B. G., Dick, G. J., Murray, K. J., Parker, D., Verity, R., and
31 Webb, S. M.: Biogenic manganese oxides: Properties and mechanisms of formation, *Annu
32 Rev Earth Pl Sc*, 32, 287-328, <https://doi.org/10.1146/annurev.earth.32.101802.120213>, 2004.
- 33 Thomsen, S., Karstensen, J., Kiko, R., Krahnemann, G., Dengler, M., and Engel, A.: Remote and local
34 drivers of oxygen and nitrate variability in the shallow oxygen minimum zone off Mauritania
35 in June 2014, *Biogeosciences*, 1-29, <https://doi.org/10.5194/bg-2018-252>, 2018.



- 1 Tomczak, M.: An analysis of mixing in the frontal zone of South and North Atlantic Central Water off
2 North-West Africa, *Prog Oceanogr*, 10, 173-192, [https://doi.org/10.1016/0079-](https://doi.org/10.1016/0079-6611(81)90011-2)
3 [6611\(81\)90011-2](https://doi.org/10.1016/0079-6611(81)90011-2), 1981.
- 4 Twining, B. S., Rauschenberg, S., Morton, P. L., and Vogt, S.: Metal contents of phytoplankton and
5 labile particulate material in the North Atlantic Ocean, *Prog Oceanogr*, 137, 261-283,
6 <https://doi.org/10.1016/j.pocean.2015.07.001>, 2015.
- 7 Ussher, S. J., Achterberg, E. P., Powell, C., Baker, A. R., Jickells, T. D., Torres, R., and Worsfold, P.
8 J.: Impact of atmospheric deposition on the contrasting iron biogeochemistry of the North and
9 South Atlantic Ocean, *Global Biogeochem Cy*, 27, 1096-1107,
10 <https://doi.org/10.1002/gbc.20056>, 2013.
- 11 Véron, A., Patterson, C., and Flegal, A.: Use of stable lead isotopes to characterize the sources of
12 anthropogenic lead in North Atlantic surface waters, *Geochim Cosmochim Ac*, 58, 3199-3206,
13 [https://doi.org/10.1016/0016-7037\(94\)90047-7](https://doi.org/10.1016/0016-7037(94)90047-7), 1994.
- 14 von Langen, P. J., Johnson, K. S., Coale, K. H., and Elrod, V. A.: Oxidation kinetics of manganese(II)
15 in seawater at nanomolar concentrations, *Geochim Cosmochim Ac*, 61, 4945-4954,
16 [https://doi.org/10.1016/S0016-7037\(97\)00355-4](https://doi.org/10.1016/S0016-7037(97)00355-4), 1997.
- 17 Wedepohl, K. H.: The composition of the continental crust, *Geochim Cosmochim Ac*, 59, 1217-1232,
18 [https://doi.org/10.1016/0016-7037\(95\)00038-2](https://doi.org/10.1016/0016-7037(95)00038-2), 1995.
- 19 Weiss, R. F.: The solubility of nitrogen, oxygen and argon in water and seawater, *Deep Sea Res and*
20 *Oceanographic Abstracts*, 17, 721-735, [https://doi.org/10.1016/0011-7471\(70\)90037-9](https://doi.org/10.1016/0011-7471(70)90037-9), 1970.
- 21 Winkler, L. W.: Bestimmung des im Wasser gelösten Sauerstoffs, *Ber Dtsch Chem Ges*, 21, 2843-
22 2855, <https://doi.org/10.1002/cber.188802102122>, 1988.
- 23 Wu, J. F. and Luther, G. W.: Size-fractionated iron concentrations in the water column of the western
24 North Atlantic Ocean, *Limnol Oceanogr*, 39, 1119-1129,
25 <https://doi.org/10.4319/lo.1994.39.5.1119>, 1994.
- 26 Wyrтки, K.: The oxygen minima in relation to ocean circulation, *Deep-Sea Res*, 9, 11-23,
27 [https://doi.org/10.1016/0011-7471\(62\)90243-7](https://doi.org/10.1016/0011-7471(62)90243-7), 1962.
- 28 Zenk, W., Klein, B., and Schroder, M.: Cape-Verde Frontal Zone, *Deep-Sea Res*, 38, S505-S530,
29 [https://doi.org/10.1016/S0198-0149\(12\)80022-7](https://doi.org/10.1016/S0198-0149(12)80022-7), 1991.

30



- 1 **Table 1.** Analyzed reference seawater, procedural blanks and detection limits (three times the standard
 2 deviation of the blank). Mean values and standard deviation for Cd, Pb, Fe, Ni, Cu, Mn and Co and
 3 available consensus values (± 1 standard deviation), n = number of measurements.

	SAFe S (nmol L ⁻¹) n=11	SAFe S consensus value (nmol L ⁻¹)	SAFe D2 (nmol L ⁻¹) n=7	SAFe D2 consensus value (nmol L ⁻¹)	Blank (pmol L ⁻¹)	Detection limit (pmol L ⁻¹)
Cd	0.003 \pm 0.002	0.001	1.089 \pm 0.043	1.011 \pm 0.024	2.2 \pm 0.3	0.8
Pb	0.050 \pm 0.003	0.049 \pm 0.002	0.028 \pm 0.001	0.029 \pm 0.002	0.4 \pm 0.2	0.6
Fe	0.091 \pm 0.009	0.095 \pm 0.008	1.029 \pm 0.038	0.956 \pm 0.024	68 \pm 10	29
Ni	2.415 \pm 0.086	2.34 \pm 0.09	9.625 \pm 0.175	8.85 \pm 0.26	112 \pm 20	59
Cu	0.514 \pm 0.037	0.53 \pm 0.05	2.176 \pm 0.152	2.34 \pm 0.15	14 \pm 3	9.3
Co	0.005 \pm 0.001	0.005 \pm 0.001	0.048 \pm 0.003	0.047 \pm 0.003	2.7 \pm 0.8	2.5
Mn	0.814 \pm 0.033	0.810 \pm 0.062	0.437 \pm 0.029	0.36 \pm 0.05	14 \pm 6	17

4

5

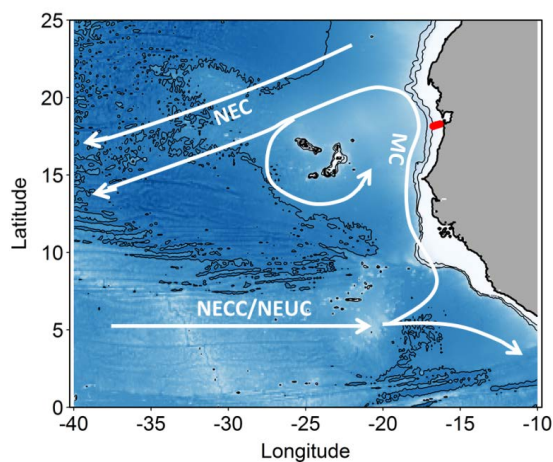


- 1 **Table 2.** TM/Al ratios of different fractions for
- 2 the repeated deployments at station 3 within the
- 3 OMZ below 50 m water depth.

Parameter	Stn 3A	Stn 3B
dFe/dAl	0.38–0.79	0.35–0.37
TDFe/TDAI	4.00–13.42	1.83–2.81
LpFe/LpAl	10.00–29.50	3.64–8.59
dCo/dAl	0.009–0.011	0.009–0.011
TDCo/TDAI	0.009–0.010	0.006–0.008
LpCo/LpAl	0.007–0.011	0.001–0.005
dMn/dAl	0.26–0.45	0.19–0.21
TDMn/TDAI	0.26–0.32	0.12–0.17
LpMn/LpAl	0.14–0.28	0.02–0.09

4

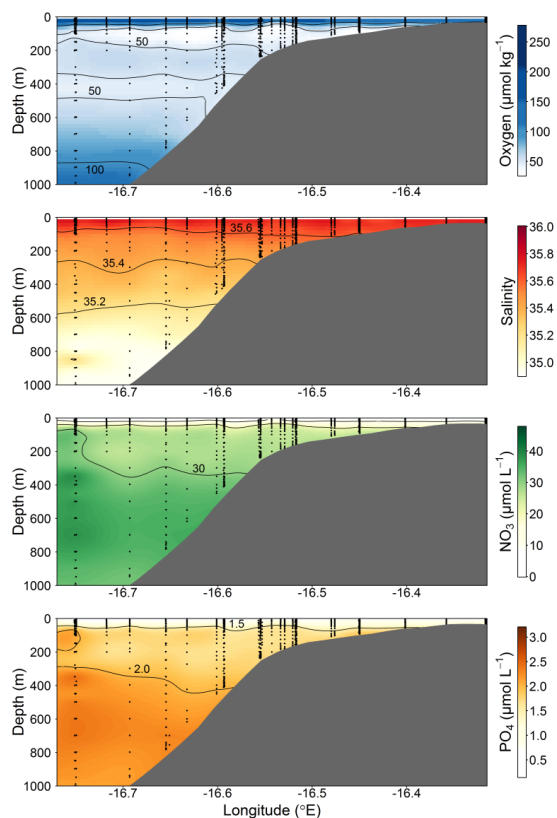
5



1

2 **Figure 1.** Map of the study area. Stations along the transect during M107 (June 2014) are displayed in
3 red circles and major currents in white lines (adapted from Brandt et al. 2015). MC = Mauritania
4 Current; NEC = North Equatorial Current; NECC = North Equatorial Countercurrent; NEUC = North
5 Equatorial Undercurrent.

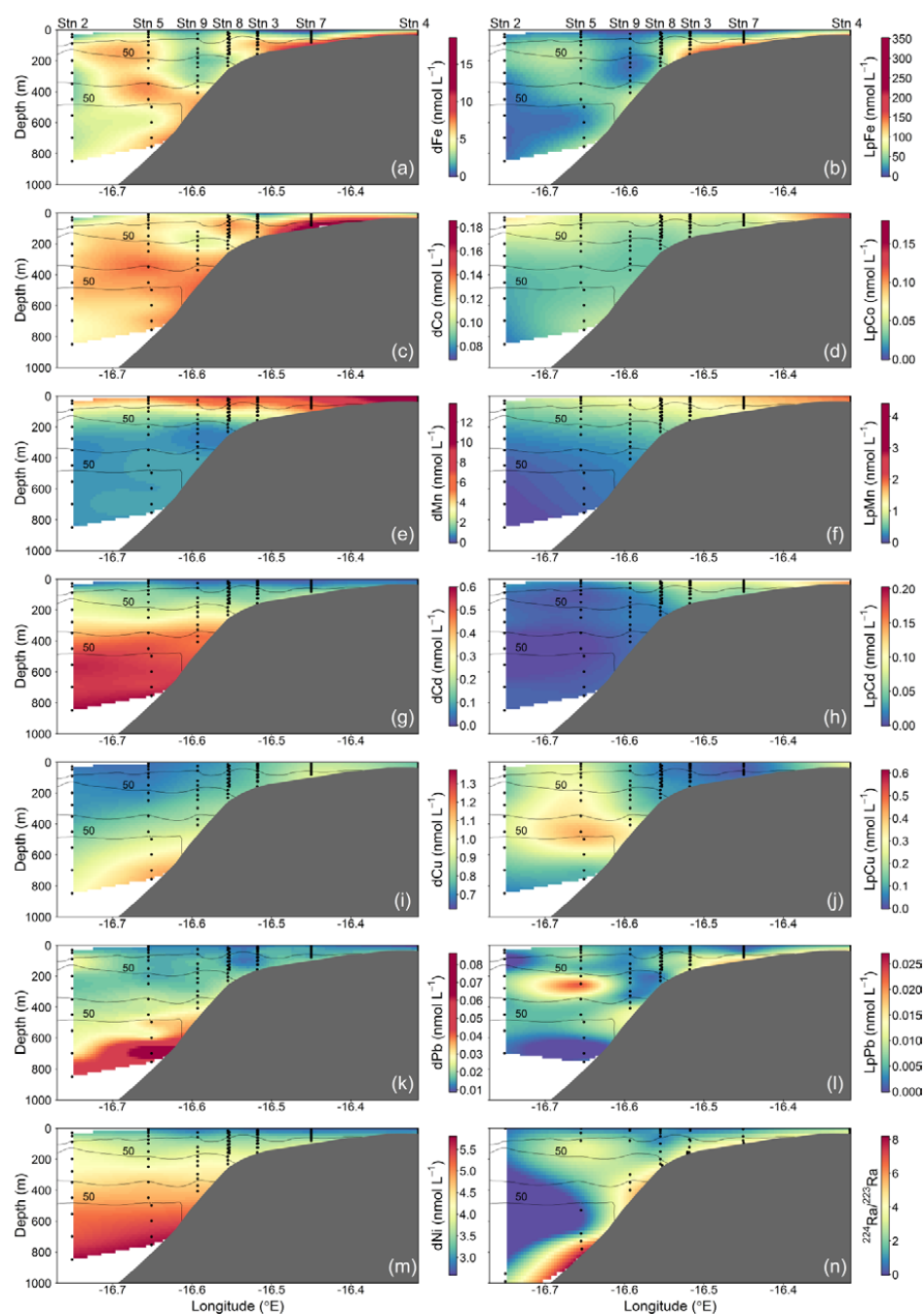
6



1

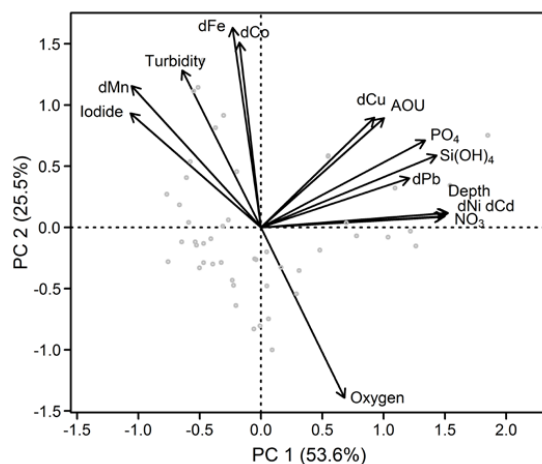
2 **Figure 2.** Section plots of oxygen ($\mu\text{mol kg}^{-1}$), salinity (PSU), NO_3 ($\mu\text{mol L}^{-1}$) and PO_4 ($\mu\text{mol L}^{-1}$)
3 along the transect off the Mauritanian coast in June 2014.

4



1

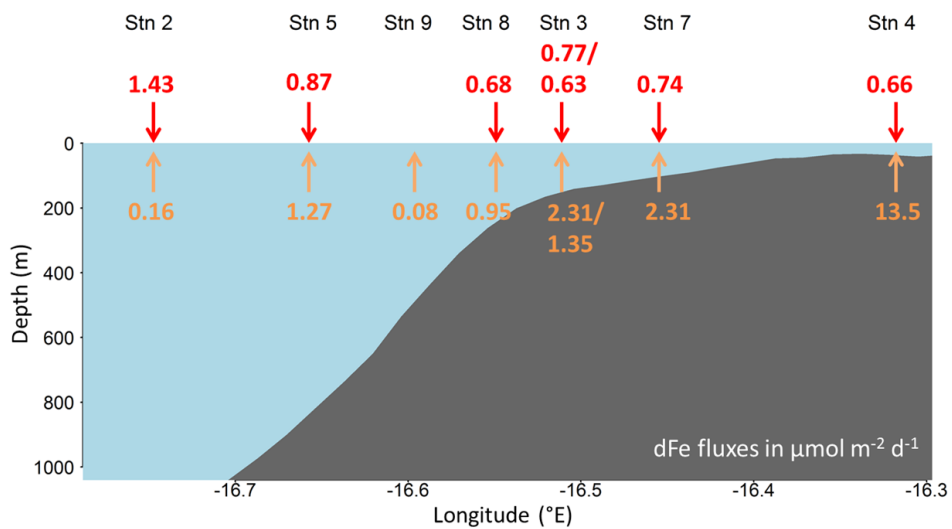
2 **Figure 3.** Spatial distributions of dissolved (d) and leachable particulate (Lp) trace metals and
 3 $^{224}\text{Ra}/^{223}\text{Ra}$ across the Mauritanian shelf at $18^{\circ}20'N$ in June 2014. Each sample location is indicated as
 4 black dot and oxygen contours at $50 \mu\text{mol kg}^{-1}$ enclosing the upper and lower OMZ are displayed as
 5 black contour lines.



1

2 **Figure 4.** Principal component analysis of the Mauritanian shelf data set. Principal component
3 loadings for each variable are indicated by black vectors. Component scores of each sample are
4 indicated as grey circles. Loadings/scores have been scaled symmetrically by square root of the
5 eigenvalue.

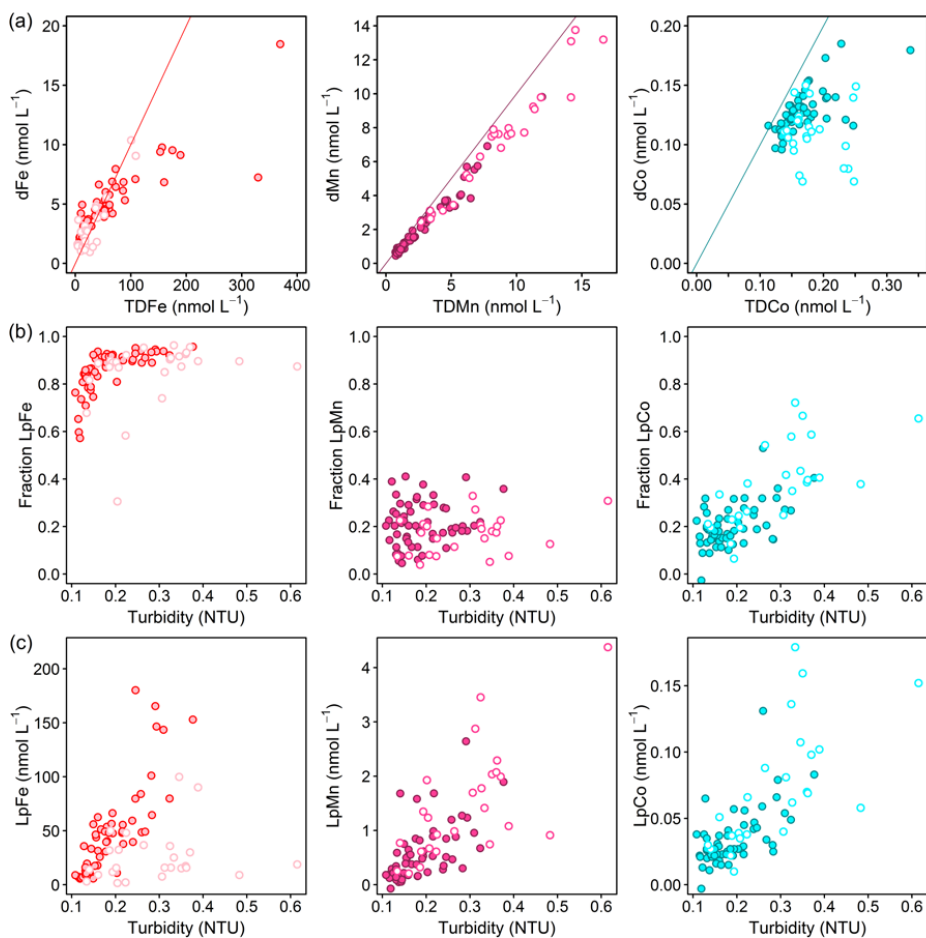
6



1

2 **Figure 5.** Atmospheric dFe fluxes (red) and vertical dFe fluxes (orange) in $\mu\text{mol m}^{-2} \text{d}^{-1}$ along the
3 transect at $18^{\circ}20' \text{N}$ in June 2014.

4



1

2 **Figure 6.** (a) Dissolved against total dissolvable trace metal concentrations for Fe (left; red line: TDFe

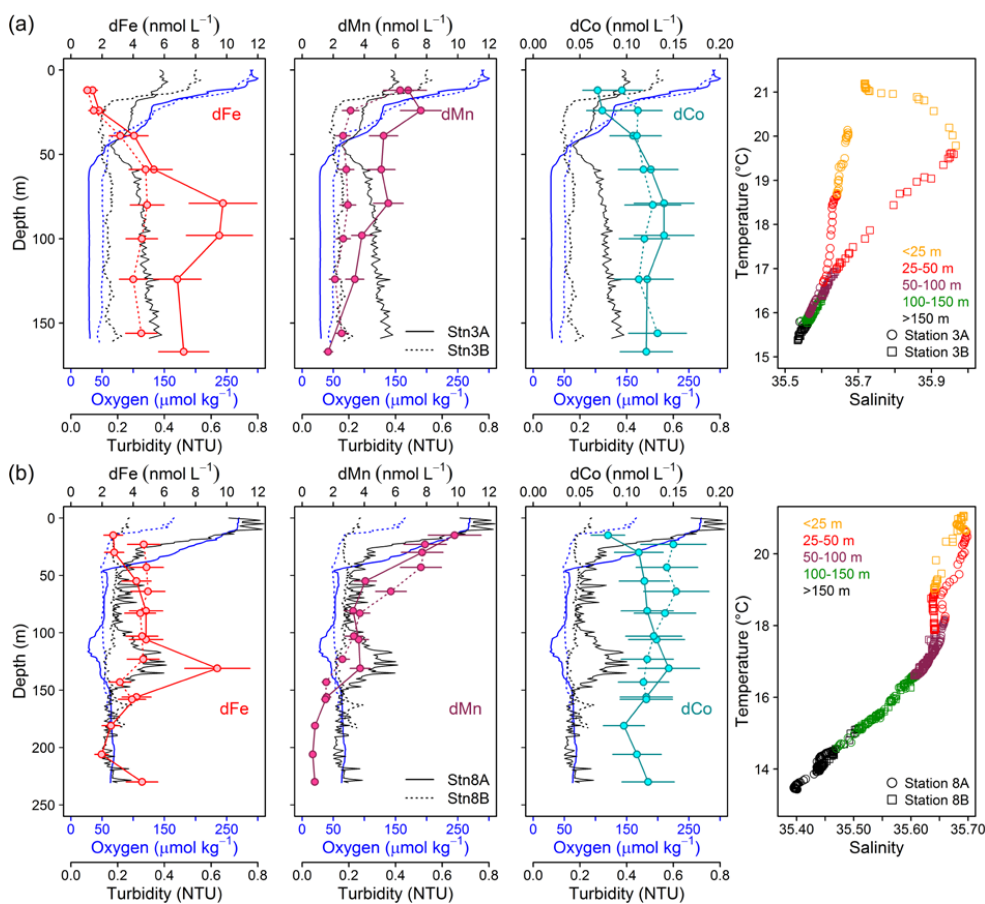
3 = 10*dFe), Mn (middle; purple line: TDMn = dMn) and Co (right; turquoise line: TDCo = dCo). (b)

4 Fraction of leachable particulate trace metals (Lp/TD) against turbidity and (c) Leachable particulate

5 concentrations against turbidity for Fe (left), Mn (middle) and Co (right). Filled circles display all data

6 points below 50 m depth, open circles at depths shallower than 50 m.

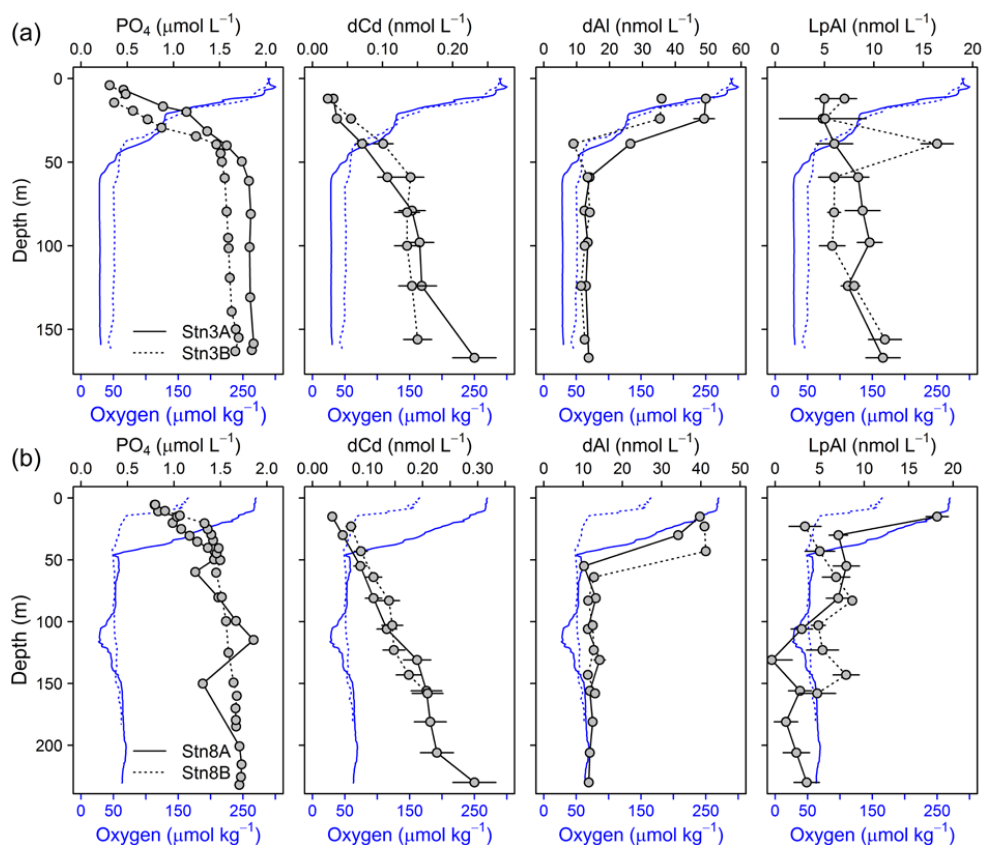
7



1

2 **Figure 7.** Repeat stations: oxygen concentration, turbidity and dissolved trace metals (Fe, Mn and Co)
 3 and temperature vs salinity plots. First deployment displayed as solid line and second deployment
 4 displayed as dashed line. (a) Station 3 (18.23°N, 16.52°W, 170 m water depth, 9 days between
 5 deployments). (b) Station 8 (18.22°N, 16.55°W, 189–238 m water depth, 2 days between
 6 deployments).

7



1

2 **Figure 8.** Depth profiles of dCd, PO₄, dAl and LpAl of repeat stations. First deployment displayed as
 3 solid black line and second deployment displayed as dashed black line. Oxygen concentrations are
 4 indicated as blue solid line for the first deployment and dashed blue line for the second deployment.
 5 (a) Station 3 (18.23°N, 16.52°W, 170 m water depth, 9 days between deployments) and (b) Station 8
 6 (18.22°N, 16.55°W, 189–238 m water depth, 2 days between deployments).

7